PHILOSOPHICAL TRANSACTIONS OF THE ROYAL SOCIETY A MATHEMATICAL, PHYSICAL & ENGINEERING SCIENCES

Graphical Modelling of Crystal Aggregates and its Relevance to Cement Diagnosis

J. A. D. Dickson

Phil. Trans. R. Soc. Lond. A 1983 **309**, 465-502
doi: 10.1098/rsta.1983.0056

Phil. Trans. R. Soc. Lond. A **309**, 465–502 (1983) [465]
Printed in Great Britain

GRAPHICAL MODELLING OF CRYSTAL AGGREGATES AND ITS RELEVANCE TO CEMENT DIAGNOSIS†

By J. A. D. Dickson
Department of Earth Sciences, University of Cambridge, Cambridge CB2 3EQ, U.K.

(*Communicated by E. R. Oxburgh, F.R.S. – Received 28 July 1982*)

[Plates 1 and 2]

CONTENTS

The identification of carbonate cements in rock sections is accomplished by means of textural criteria. Some of these criteria, relating to crystal fabric, may be modelled graphically in crystal growth diagrams.

Existing crystal growth diagrams are oversimplified. Three new crystal growth

† Cambridge Earth Science Series ES 338.

diagrams are presented for calcite $\{10\bar{1}1\}$, $\{40\bar{4}1\}$ and $\{01\bar{1}2\}$ rhombohedra. The crystals are envisaged as growing by zones of equal width from an inert substrate. The patterns that growth zones create on cuts through individual crystals are used as templates to produce the crystal growth diagrams. 151 crystals seeded on the substrate, on both sides of the crystal growth diagram, are considered to grow at identical rates and impinge on one another.

The three crystal growth diagrams illustrate features of crystal initiation and shape in two dimensions not found in previously published diagrams. The rate of maturation of the crystal fabric away from the substrate is shown to depend partly on crystallographic form. Optical elongation is also shown to be related to crystallographic form. The enfacial junction, a special type of triple junction, is shown to be absent from the crystal growth diagrams.

The diagrams presented are constrained. Changes in (i) the direction of crystal cutting, (ii) crystallographic form during growth, (iii) the number of crystallographic forms at one time, (iv) the positioning of nuclei, (v) shape of the substrate, and (vi) the change to an active substrate where epitaxy occurs, would all change the character of the crystal growth diagram.

The technique of using a list of textural criteria for identifying cements is rejected. Such lists may be used to identify the morphological type of crystal aggregate. After examination of other properties, the decision as to whether that type of aggregate is cement or not can be made.

The recognition of impingement growth is made easy if all stages of maturation are present. Where insufficient space is available for mature growth to develop, recognition must rely on features other than textural. A calcite aggregate developed in a Permian bryozoan biolithite is used to illustrate immature impingement growth. This aggregate is identified as of impingement type principally from the arrangement of growth zonation shown in each crystal by cathodoluminescence.

The enfacial junction, often regarded as the least equivocal criterion for the recognition of cements, is absent from the crystal growth diagrams and the Permian biolithite. The origin of enfacial junctions in a Lower Carboniferous spar is thought to be due either to unusual sporadic growth inhibition or, more likely, to intercrystalline boundary migration due to dissolution. Enfacial junctions are common in ancient spars: if generated by intercrystalline dissolution considerable quantities of $CaCO_3$ have been liberated. Enfacial junctions also develop at the junction of two generations of crystals not exhibiting epitaxy.

1. Introduction

The growth of crystals from a substrate into a liquid-filled cavity (i.e. cementation) is a common natural phenomenon. Direct observation while growth proceeds is a satisfactory method of investigating such crystal aggregates, but often this is impractical. The genesis of a crystal aggregate is usually interpreted from the pattern of intercrystalline boundaries displayed on slicing the aggregate, that is to say, the three dimensional history of crystal growth is deduced from a two-dimensional slice, which is a difficult stereological exercise. In the past, to aid in this interpretation, graphical models have been constructed which show growth zones or time lines in addition to the intercrystalline boundaries.

A work of central importance to an understanding of the growth of crystal aggregates is Buckley's (1951) book *Crystal growth*. Buckley described and illustrated (figure 87) how crystals growing in a confined space, with their greatest linear crystallization velocities unfavourably oriented with respect to the growth space, were 'crowded out' or overhauled by more favourably oriented crystals. The most favourable orientation is with the greatest linear crystallization velocity (subsequently termed *greatest growth vector*, g.g.v. in this paper) oriented

PHILOSOPHICAL TRANSACTIONS OF THE ROYAL SOCIETY A MATHEMATICAL, PHYSICAL & ENGINEERING SCIENCES

normally to the substrate. He also described and illustrated (1951, figure 89) the development of columnar crystals, due to this same selection of (metal) crystals, in cylindrical or rectangular castings.

The application of Buckley's work is wide, but only its use in the study of carbonate cements and mineral veins is considered here. The most critical work on the recognition of carbonate cements is Bathurst's (1958) paper, which was enlarged by him in 1971 into a list of criteria for the diagnosis of cement. A similar list was incorporated by Bricker (1971) in the book *Carbonate cements* (p. 149) and has been reiterated by Chilingar *et al.* (1979), and many others. Carbonate petrographers strive to distinguish calcite aggregates precipitated onto a substrate from solutions and that grow into open spaces in a strain-free environment, that is, cements, from those aggregates generated by recrystallization or replacement of a solid precursor. The lists of criteria referred to above form the mainstay of cement recognition in carbonate rocks. Bathurst (1971) pointed out that the criteria used for the recognition of cements can be grouped into two sets. One is concerned with spatial arrangement of the crystals, for example, they should occupy an area which was previously fluid-filled. To use this set of criteria, the research worker requires experience. The second set of criteria is intrinsic to cement and relates to the fabric of the polycrystalline mass. Four of the five criteria in the second set are:

(1) plane intercrystalline boundaries,
(2) crystal size increases away from substrate,
(3) preferred orientation of longest axes normal to substrate, and
(4) preferred orientation of optic axes normal to substrate.

These may be related to crystal growth diagrams. The fifth criterion, the enfacial junction, is a triple junction where one angle is 180°. This was introduced by Bathurst in 1964, and was regarded by him (1971) as one of the least equivocal criteria for the recognition of cement. In practice, however, many petrographers recognize cements using the first set of criteria, which is surprising since the second set is more objective. This second set, considered intrinsic to cements, is commonly, inexplicably, absent from some crystal aggregates interpreted as cement. This dilemma is explored in what follows and it is shown that no combination of fabric criteria is uniquely diagnostic for cements.

The generation of plane intercrystalline boundaries was explained by Schmidegg (1928), who produced the first crystal growth diagrams for carbonate minerals. Criteria 2 and 3, in the above list, can be traced to Buckley's work. Grigor'ev's work (1965) has escaped attention; not only did he produce crystal growth diagrams (1965, particularly figure 168), but he also proposed three growth stages in the development of a crystal aggregate. The first growth stage is one of separate crystals, developed by outward extension of crystal faces from their nucleation points until faces of adjacent crystals meet. The size to which the crystals develop during this stage depends on nuclear spacing. Intercrystalline boundaries appear in the second stage which Grigor'ev termed the drusy stage: during this all crystals with their g.g.vs not oriented normally to the substrate are eliminated. The third and final stage is one of parallel-columnar growth, where the morphology of the crystals remains constant, unless the status of the g.g.vs is changed. There is no clear-cut dividing line between the three stages, the change from one stage to another is not synchronous.

Crystal growth diagrams, to date, have been produced to illustrate particular features of growth and are very constrained. Each diagram is constructed using exactly the same cut

through all its component crystals. The crystals are all nucleated on the line of intersection between the substrate and the plane of the crystal growth diagram. The diagrams presented here do not have these constraints. The component crystals are cut by the plane of the diagram in three different orientations, and 151 substrate nuclei are considered to be at varying distances from the line of intersection between substrate and crystal growth diagram. As with previous diagrams, the crystals are envisaged as growing by zones or increments of equal width, measured normally to each crystal face. The substrate is passive (no epitaxy occurs) and is plane, so the diagrams find a close natural analogue in parallel, plane-sided veins, where the fill grew from randomly distributed nuclei on both walls, and met along a median commissure.

The new diagrams were constructed not only to produce a more realistic model of crystal growth, but also to investigate the effects that differing crystallographic form might have on the ensuing crystal aggregate. The complexity of graphical construction for a diagram composed of 151 crystals is considerable, so the crystallographic form was kept to the simplest closed form – the rhombohedron. Crystallographic data are available for the three calcite rhombohedra modelled (Palache *et al.* 1951), which frequently crystallize naturally on the walls of liquid-filled cavities. The Miller–Bravais system of crystallographic notation is used throughout this paper.

The crystal growth diagrams presented here model a particular type of crystal growth. The criteria used to identify this type of impingement aggregate are refined by these models, but such criteria should not be used to diagnose cement in isolation from other considerations. Impingement aggregates do form by replacement, for example, dolomite which replaces calcite is usually idiomorphic until adjacent crystals meet and then impingement texture develops. Nuclei of such replacive dolomite crystals are usually scattered throughout the calcite host, so the type of impingement texture is unlike that modelled here. However, if dolomite nucleation is confined to a surface, then replacive growth away from the substrate would result in impingement textures having the characteristics displayed by the crystal growth diagrams presented here (Fairchild 1980).

Folk (1965) has described calcite recrystallization from surfaces that yield an aggregate with all the features of normal pore-filling spar. This material he termed pseudospar, and he emphasized that any process (precipitation or recrystallization) starting from a surface and progressing outward should yield the same product. However, many examples of recrystallized or neomorphic calcite show initiation at scattered points and the crystals rarely grow by the development of regular crystal faces. Impingement texture in recrystallized calcite appears to be rare.

The subject of crystal growth diagrams is treated here in the following way. First, the patterns that growth zones create on cuts through individual crystals are considered. These unique patterns are then used as templates from which crystal growth diagrams are constructed. Secondly, the relevance of these diagrams, particularly to the diagnosis of calcite cements, is discussed.

2. Perspective diagrams

The pattern of growth zonation on a cut that passes through the centre of a crystal is relatively easy to visualize. Growth zonation on cuts away from the centre is difficult to picture, especially if the direction of cut does not include any element of the crystal's symmetry. To illustrate some of these features, perspective views of cuts through a $\{10\bar{1}1\}$ rhombohedron possessing eight growth zones are shown in figure 1. In this figure, the cuts are vertically

oriented, parallel to the c-axis and normal to the $(10\bar{1}1)$ face. Four cuts are shown, one (labelled 0) passing through the crystal's centre, and three (labelled i, ii, and iii) cutting the crystal progressively further away from the centre. The cut which passes through the crystal's centre displays all eight concentric growth zones, but, with increasing distance of the cut from the centre, the earlier zones are progressively omitted. The angular relationships of each zone in all cuts are identical. The shape of each zone in the central cuts is identical, but the shapes of

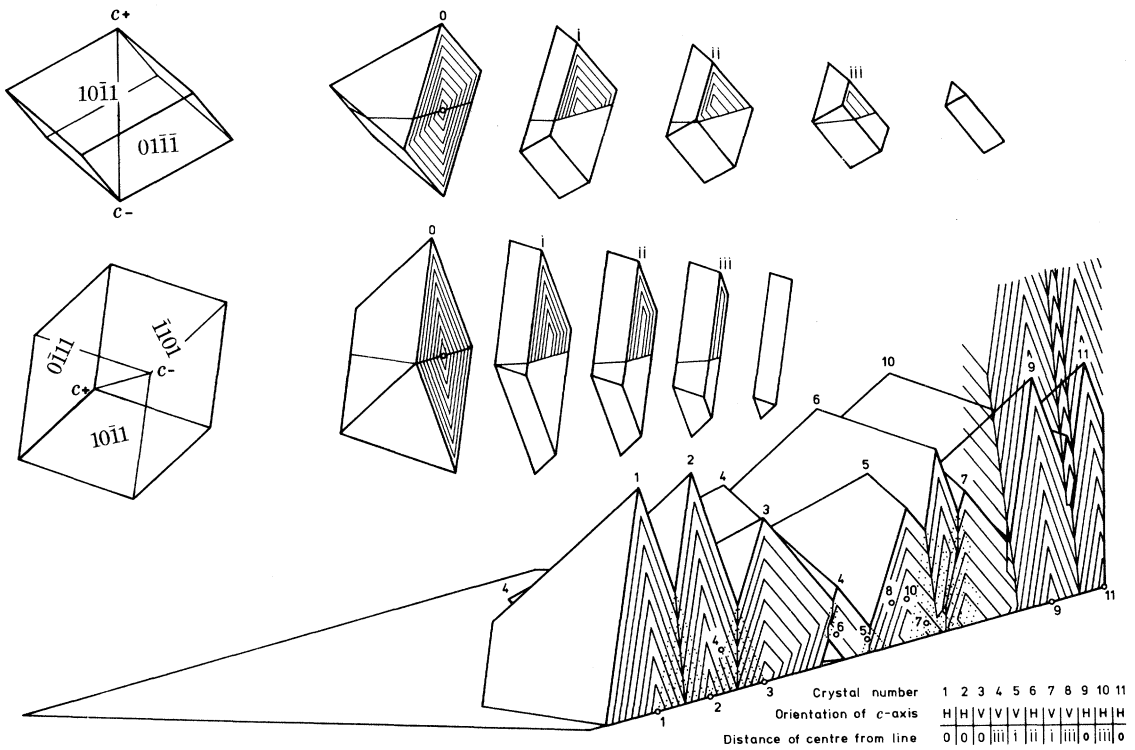

FIGURE 1. Vertical cuts through $\{10\bar{1}1\}$ rhombohedron and the use of growth patterns on those cuts to produce a crystal growth diagram. *Top row left*: $\{10\bar{1}1\}$ rhombohedron viewed in conventional crystallographic position with the c-axis vertical and $(10\bar{1}1)$ face towards observer. *Top row right*: exploded segments of rhombohedron showing how eight equal growth zones intersect four vertical cuts (0, i, ii and iii). Vertical cuts taken normally to $(10\bar{1}1)$ face, or towards observer. *Middle row*: identical to top row except that the $\{10\bar{1}1\}$ rhombohedron and segments are viewed with the c^+-axis horizontal, pointing towards observer. *Lower diagram*: perspective view of crystal growth diagram, which is a slice taken normally to the substrate. The c-axis orientation of the crystals is shown at lower right as either H = horizontal (parallel to substrate) or V = vertical (perpendicular to substrate). The distance of the crystal's centre or nucleus from the line in the horizontal plane is also shown at lower right; the line referred to is the line of intersection between the substrate and the plane of the crystal growth diagram. In the lower diagram the templates used to draw the zones of crystals 1–7 are shown dotted where they overlap. Overlapping zones of crystals 7–11 are not shown, but 7 additional growth zones are projected above growth zone 8 to show how the pattern may be extrapolated.

zones in cuts away from the centre differ. The series of cuts in the upper row of figure 1 is taken from a crystal orientated in the conventional crystallographic position with the c-axis vertical and the $(10\bar{1}1)$ face towards the observer. The series of cuts shown in the middle row of figure 1 is taken from an identical $\{10\bar{1}1\}$ rhombohedron, but the c^+-axis is tilted 90° towards the observer so that it lies horizontally. The distances between any two cuts in either the upper or middle rows are identical.

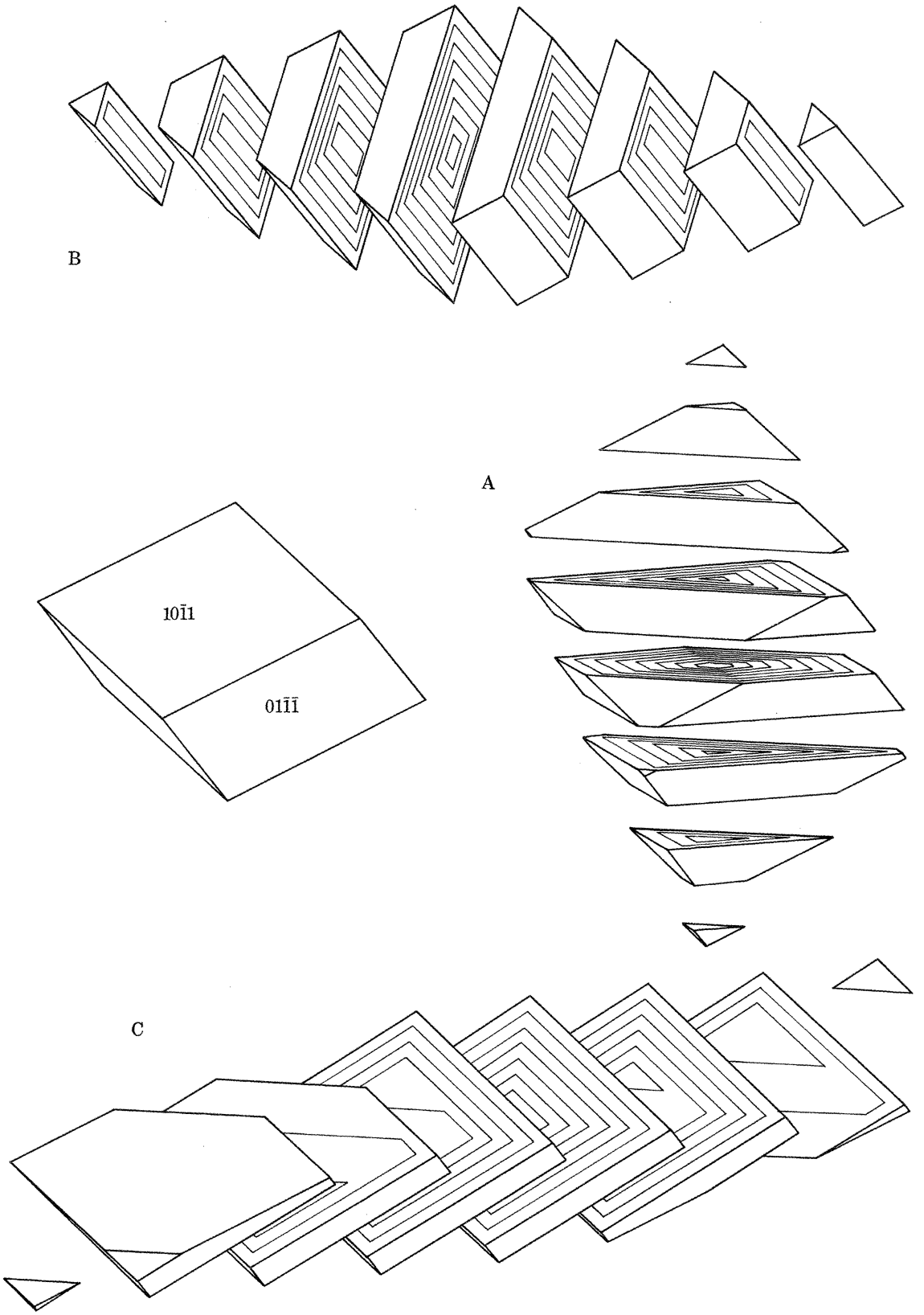

FIGURE 2. Projection of $\{10\bar{1}1\}$ rhombohedron. *Centre left*: entire $\{10\bar{1}1\}$ rhombohedron. *Series* A: Eight exploded segments of $\{10\bar{1}1\}$ rhombohedron created by 7 horizontal cuts coincident with the (0001) plane. *Series* B: Eight exploded segments of $\{10\bar{1}1\}$ rhombohedron created by 7 vertical cuts oriented normally to the $(10\bar{1}1)$ face (same direction as that used in figure 1). *Series* C: Eight exploded segments of $\{10\bar{1}1\}$ rhombohedron created by 7 cuts oriented E–W or 90°/270°, and tilted towards observer at 60° to the horizontal.

PHILOSOPHICAL TRANSACTIONS OF THE ROYAL SOCIETY A MATHEMATICAL, PHYSICAL & ENGINEERING SCIENCES

The apparent differences in zonal shapes between the two rows of cuts in figure 1 are caused by perspective; if cuts of the same number are viewed normally, the zonal pattern would be identical.

The visualization of the growth zone patterns in a cut through an individual crystal may be a difficult mental exercise. The patterns produced where several crystals impinge are impossible to picture, but they may be constructed. Such a construction is shown in the lower right portion of figure 1, where eleven crystals are considered to have grown from point nuclei on a plane substrate with their *c*-axes either parallel or normal to the substrate. The plane shown in figure 1, which is normal to the substrate, and against which all eleven crystals impinge, is the crystal growth diagram. By arranging the eleven nuclei in a particular way, the 0, i, ii and iii cuts shown in the middle and upper rows of figure 1 may be used as templates to produce the lower diagrams. The *c*-axes of crystals 1, 2, 6, 9, 10 and 11, in addition to being parallel to the substrate, are also parallel to the plane of slice. Five crystals, 1, 2, 3, 9 and 11, have their nuclei on the line of intersection between the substrate and the diagram and show all eight growth zones. Six crystals 4, 5, 6, 7, 8 and 10 have their nuclei behind the plane of the diagram and consequently show less than 8 growth zones.

The construction of simple perspective drawings, such as those shown in figure 1, greatly assists in cognition, but the arrangement and orientation of nuclei are constrained by the difficulty of producing such figures and hence oversimplification results. Despite this oversimplification, figure 1 illustrates two features not included in previous literature. First, crystals may enter the plane of the crystal growth diagram above the substrate (crystals 6, 8 and 10, figure 1). These crystals *are* initiated on the substrate, but away from the plane of the diagram into which they grow. Secondly, growth may be directed towards the substrate. This is illustrated by the 'tunnel' beneath crystals 3 and 4, which would, with continued growth, be occluded by growth towards the substrate.

The plane of the diagram shown in the lower part of figure 1 would be unrealistic for use as a model for crystal growth because the arrangement of crystals is too constrained. A greater degree of freedom is necessary both in the directions of crystal cuts, and in the orientations of the derived templates, before a diagram can be produced which is suitable as a model for polycrystalline growth textures. Three widely differing directions of crystal cutting are considered adequate to show all the major features of intergrowth in a crystal growth diagram and are few enough to facilitate construction. The cuts used here are illustrated in figure 2. The central cut in each of the A, B or C series in figure 2 passes through the crystal's centre and displays concentric zones of identical shape. Each cut taken away from the centre displays a sequence of zones that commonly show dramatic differences in shape; particularly marked in the C series of cuts.

3. Crystal growth diagrams

(*a*) *Construction of templates*

Figures 1 and 2 help in visualizing the stereology of crystal cutting, but the true shapes and dimensions of the growth zones are distorted by perspective. A two-dimensional crystal growth diagram may be constructed from templates if the pattern of growth zones, viewed normally to the cut, is known. The construction of such templates requires two sets of data; the interfacial angles between crystal faces in the plane of the cut, and the apparent width of the growth

zones in the plane of the cut. These data are readily derived by stereographic projection of the crystal form being considered.

The apparent angle between two faces in the plane of the cut is determined as follows. A stereogram is constructed using an upper hemisphere projection showing the crystal faces as planes, and the plane of the cut or random plane. When the random plane is a great circle, the apparent interfacial angle is that between the intersection of the two crystal faces on the random plane. This is illustrated in figure 3A where the angle between the $(\bar{1}101)$ and $(0\bar{1}11)$ faces in the random plane (C-cut direction) is 105°.

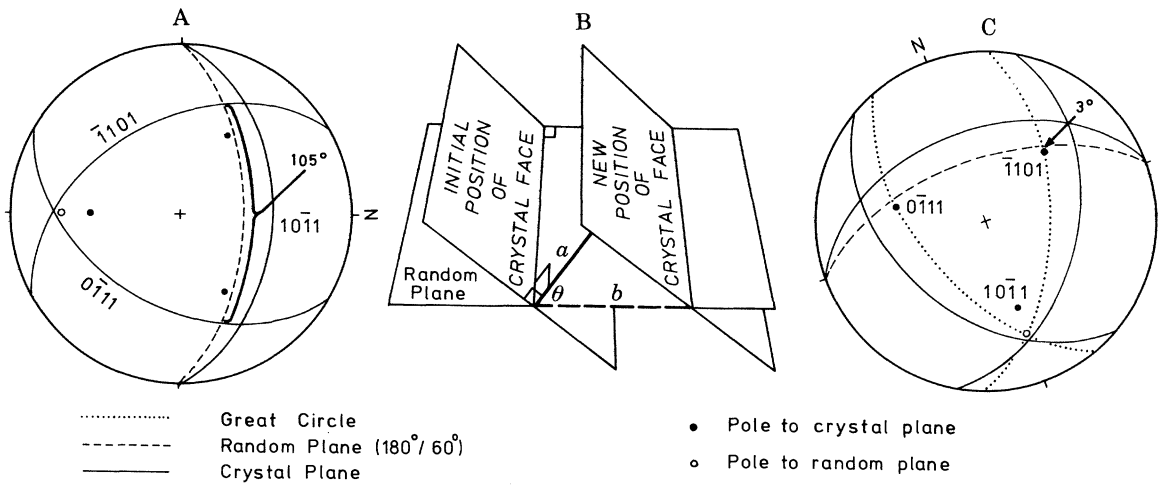

FIGURE 3. A. Stereogram illustrating how an interfacial angle on a random plane may be determined. The zero position on the primitive circle is marked N. The random plane is tilted 60° towards 180° (Cut C of figure 2). The interfacial angle shown, 105°, is between the $(\bar{1}101)$ and $(0\bar{1}11)$ faces of the $\{10\bar{1}1\}$ rhombohedron. B. Projection showing two positions of a crystal face and their intersection with a random plane. The distances a and b, and the angle θ, involved in calculating the apparent width between the two positions of the face and the random plane are shown. C. Stereogram illustrating a specific example of situation B and the determination of angle θ. The required angle, that between a line normal to the $(\bar{1}101)$ face and the random plane (cut C of figure 2), is 3°.

The relationship between the apparent width of a growth zone in the random plane and its true width is shown in figure 3B. The distance a is the true width or thickness of the growth zone, which throughout this work is set at unity. Distance b is the apparent width that is required to produce the templates:

$$b = a \sec \theta.$$

FIGURE 4. The arrangement of eight equal growth zones displayed on cuts through the $\{10\bar{1}1\}$ rhombohedron. These cuts are shown in perspective in figure 2, but here they are viewed normally to the cut surface. Each image may be used as a template to construct crystal growth diagrams, as illustrated in figure 1. When constructing these models, if the crystal's nucleus is sited on the line of intersection between the substrate and the crystal growth diagram a central template is used (labelled 'centre on line'). If the nucleus is in front of the plane of the crystal growth diagram a template labelled 'in front' is used. If the nucleus is behind, a template labelled 'behind' is used. Templates away from a central cut show a succession of forms: protomorph, mesomorph and holomorph. With 1.00 as the width of a growth increment or vector measured normally to two consecutive zones, the numerical value of various growth vectors are listed at the base. Growth vector 6 under column C does not appear on the template illustrated, but lies between the most acute angles of two consecutive protomorphic images. Vector 1 under column C is not normal to a face. The value is slightly greater than unity but has been rounded. Further details are to be found in the text. ●, Point where line from centre normal to plane of slice intersects 'template'; ○, centre.

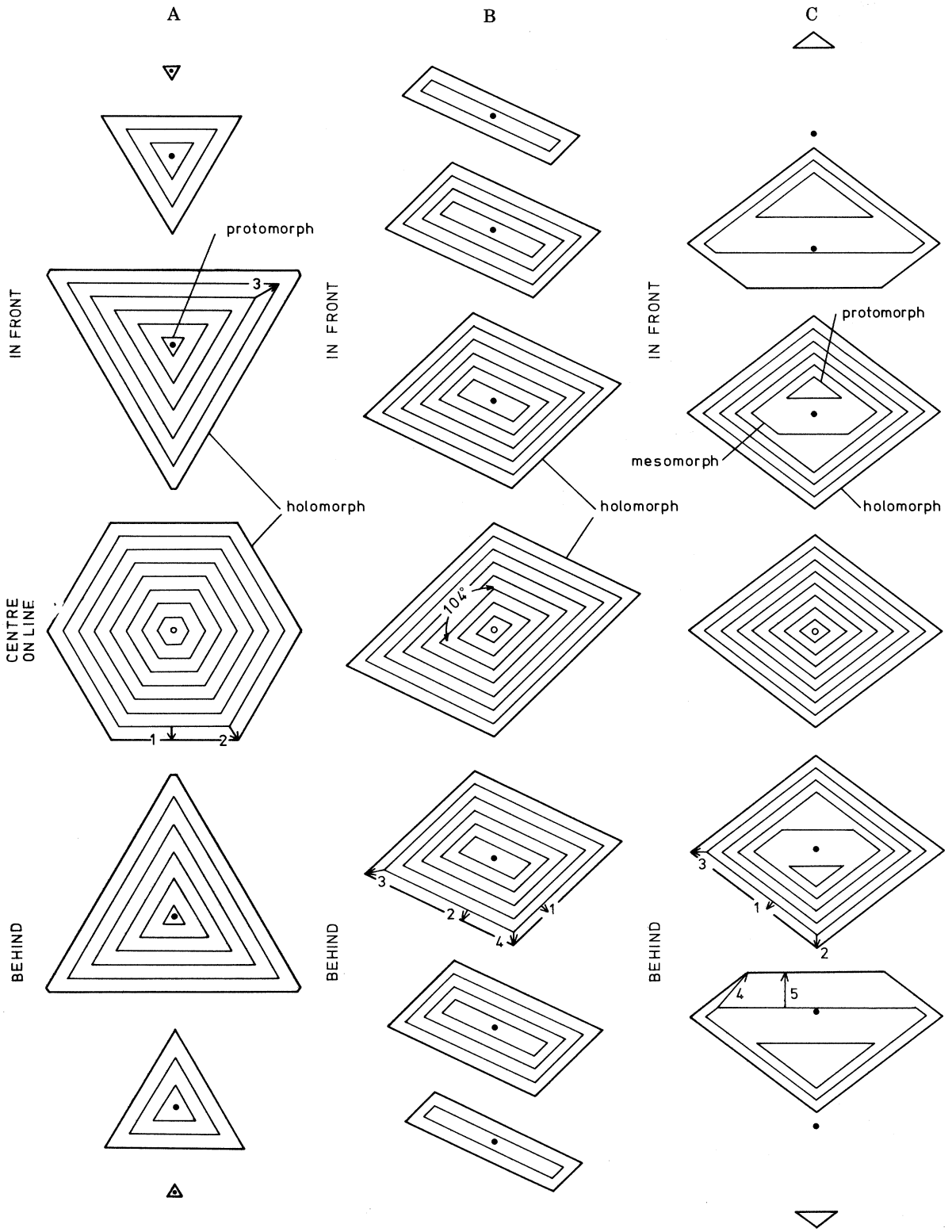

growth vectors

A		B		C	
1, 1.42	2, 1.64	1, 1.00†	2, 1.25	1, 1.00	2, 1.28
3, 2.85		3, 1.97‡	4, 1.39	3, 1.65	4, 4.94
				5, 3.74	6, 7.51

† Increment normal to face; ‡ greatest growth vector.

FIGURE 4. For description, see opposite.

Angle θ is found from a stereogram as follows. The pole to the crystal face and the pole to the random plane are placed on a great circle. The angle between the pole to the crystal face, and the random plane (angle θ) is measured along the great circle. In figure 3C, the angle between the pole to face $(\bar{1}101)$ and the random plane is 3°.

(*b*) *Rhombohedral templates*

The templates shown in perspective in figure 2 are displayed in figure 4, but viewed normally to the cut surfaces. These templates are later used to construct a two-dimensional crystal growth diagram in a similar way to that illustrated in perspective in figure 1. Crystals whose centres or nuclei are sited on the line of intersection between the substrate and the crystal growth diagram will, when cut, produce templates such as those shown in the centre of the A, B and C columns of figure 4 (labelled centre on line). The shape of each concentric growth zone in any one of these central templates is identical. If, however, the crystal nuclei are sited on the substrate in front or behind the plane of the crystal growth diagram, then the shape of consecutive growth zones will not remain constant. Examples of changing growth zone patterns for such cuts are also shown in figure 4. In these images a succession of differently shaped zones is displayed. In the C series of cuts, the simplest triangular growth zone occurs in the core of the template. This is followed by a 5-sided and finally a 4-sided figure. The 4-sided figure is identical in shape to any of the zones developed in the central template of column C. It is proposed here to name these forms for reference purposes.

In a single direction of crystal cutting, all templates will eventually develop a common growth zone shape which is identical to all growth zones on the central template; such a form is termed the *holomorph*. In cuts away from the crystal's centre, the most proximal growth zone is the *protomorph*. The protomorph may have an eccentric position relative to the distally developed holomorph (see column C, figure 4). The term *mesomorph* is used here for an intermediate form between the protomorph and holomorph and other terms (such as oligomorph, etc.) can be coined for additional forms as required. Any single cut direction will show an invariant sequence of forms. This succession of growth zone forms or figures seen in two dimensions can erroneously be interpreted as a change in crystal form (or habit) during growth.

Growth vectors can be measured between any two growth zones on a particular template. The largest growth vectors (shown in figure 4) apply to protomorphic zones, but it should be remembered that not only are these ephemeral forms which ultimately give way to holomorphic zones, but also these are apparent growth vectors which are only significant in the two dimensions of the template's cut. In three dimensions, the width between two growth zones is set at unity in this work, and the g.g.vs occur in the most acute corners (or coigns) of closed crystallographic forms, such as the $\{10\bar{1}1\}$ rhombohedron (Buckley 1951). The true width between growth zones of the $\{10\bar{1}1\}$ rhombohedron is shown in the B templates (growth vector 1, figure 4B), for this cut direction intersects the $(10\bar{1}1)$ and the $(\bar{1}01\bar{1})$ faces normally. The B template also passes through two of the six most acute coigns of the rhombohedron, so it also contains two of the six g.g.v's (growth vector 3, figure 4).

One aim of this work is to investigate how crystallographic form may affect the structure of crystal aggregates. To this end, two other crystal growth diagrams are presented using the acute $\{40\bar{4}1\}$ and the obtuse $\{01\bar{1}2\}$ rhombohedra. The templates for these additional diagrams are shown in figures 5 and 6. Identical positioning of the A, B and C cut directions and an identical growth zone width is used for all 3 sets of templates (direct comparison of template

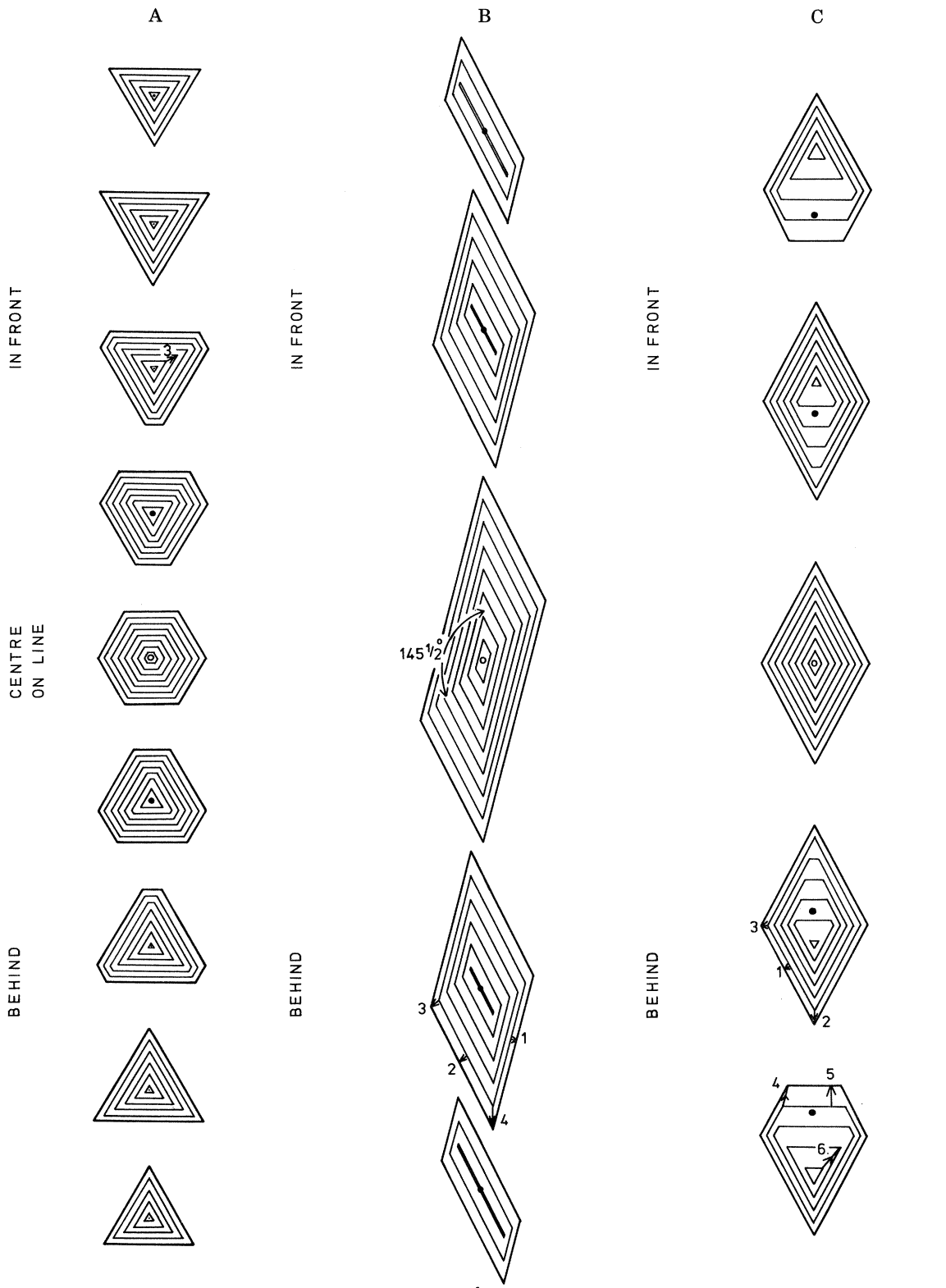

growth vectors

A		B		C	
1, 1.03	2, 1.19	1, 1.00†	2, 1.83	1, 1.05	2, 2.23
3, 2.06		3, 1.92	4, 4.08‡	3, 1.19	4, 3.70
				5, 3.63	6, 4.80

†Increment normal to face; ‡Greatest growth vector.

FIGURE 5. The arrangement of eight equal growth zones on cuts through the $\{40\bar{4}1\}$ rhombohedron. The distances between all crystal cuts are identical with those in figures 4 and 6. The format of this diagram is similar to figure 4 except that a different number of cuts are considered in the A, B and C template rows. ●, Point where line from centre normal to plane of slice intersects 'template'; ○, centre.

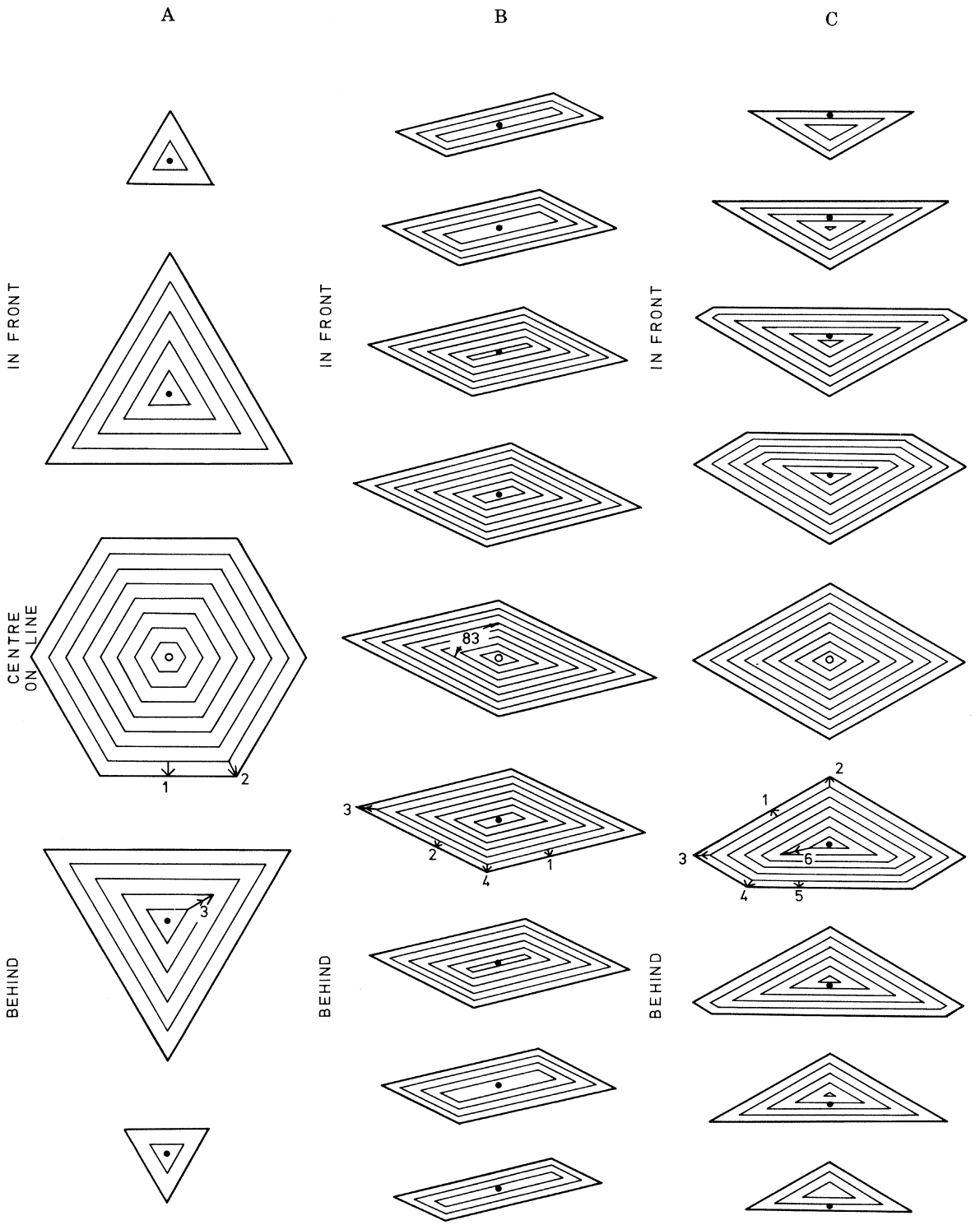

A		B		C	
growth vectors					
1, 2.28	2, 2.64	1, 1.00†	2, 1.08	1, 1.30	2, 1.52
3, 4.57		3, 3.04‡	4, 1.12	3, 2.61	4, 1.32
				5, 1.00	6, 4.44

† Increment normal to face; ‡ greatest growth vector.

FIGURE 6. The arrangement of eight equal zones on cuts through the $\{01\bar{1}2\}$ rhombohedron. The distances between all crystal cuts are identical with those in figures 4 and 5. The format of this diagram is similar to figure 4 and 5 except that a different number of cuts is considered in the A, B and C template rows. Vector 5 under column C is not normal to a face. The value is slightly greater than unity but has been rounded. ●, Point where line from centre normal to plane of slice intersects 'template'; ○, centre.

PHILOSOPHICAL TRANSACTIONS OF THE ROYAL SOCIETY A MATHEMATICAL, PHYSICAL & ENGINEERING SCIENCES

sizes between figures 4, 5 and 6 cannot be made because they are presented at different scales). The difference in template symmetry between figures 4 and 5, and figure 6 is caused by the $\{01\bar{1}2\}$ rhombohedron (figure 6) being a negative form, whilst the $\{10\bar{1}1\}$ and $\{40\bar{4}1\}$ forms are positive rhombohedra.

(*c*) *Arrangement of nuclei*

The positions of 151 numbered nucleation points on the substrate from which the crystal growth diagrams or models are constructed are shown in figure 7. Figure 7 is a plan view of the substrate, so the crystal growth diagram or the model plane appears as a straight line; nuclei 1–5 occur along this line. Nuclei 6–9 occur behind the line and nuclei 10–13 form another row an identical distance in front of the line. The numbers allocated to each row of nuclei increases with increasing distance from the model plane. Each nucleation point is assigned an A, B or C cut direction, which in turn determines the pattern of growth zones or the template to be used on the model plane. The templates have one degree of freedom. They may rotate in the plane of the model. A unique direction is required on the template so that its orientation can be

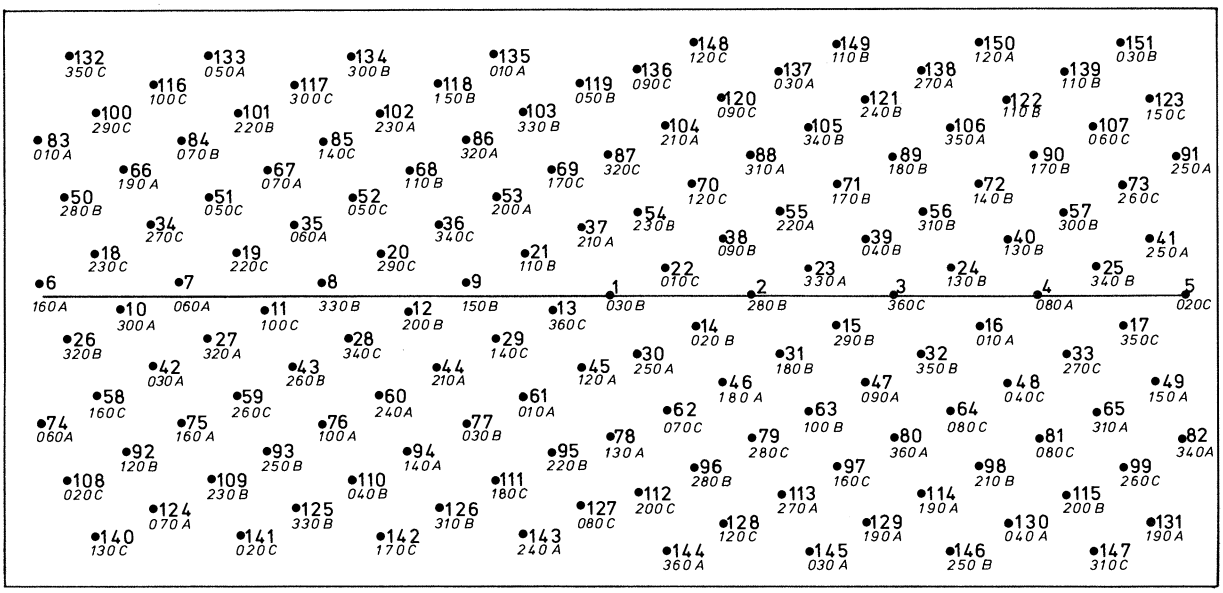

FIGURE 7. Plan view of substrate showing distribution of 151 nucleation points. Crystal growth diagram or model plane is shown as a line. Each nucleation point is assigned an A, B or C direction of cut and a template orientation. Further details are to be found in the text.

specified. The direction of the c^+ axis on the template is used for this purpose in the B and C templates, and in the horizontal A template the 360°/000° direction, or that directly away from the observer, is used. In figures 4, 5 and 6 the templates are all presented with this unique direction uppermost. These directions allow each template to be placed in one of 36 possible positions, a complete rotation being divided into 10° classes. The cut and template orientation is given, both of which were selected on a random basis, below each nucleus number on figure 7.

(*d*) *Arrangement of templates*

The relation between the nucleation point of a crystal and the choice of template is shown in figure 8. Here the horizontal substrate is viewed from the west (or left). At eye level, the plane

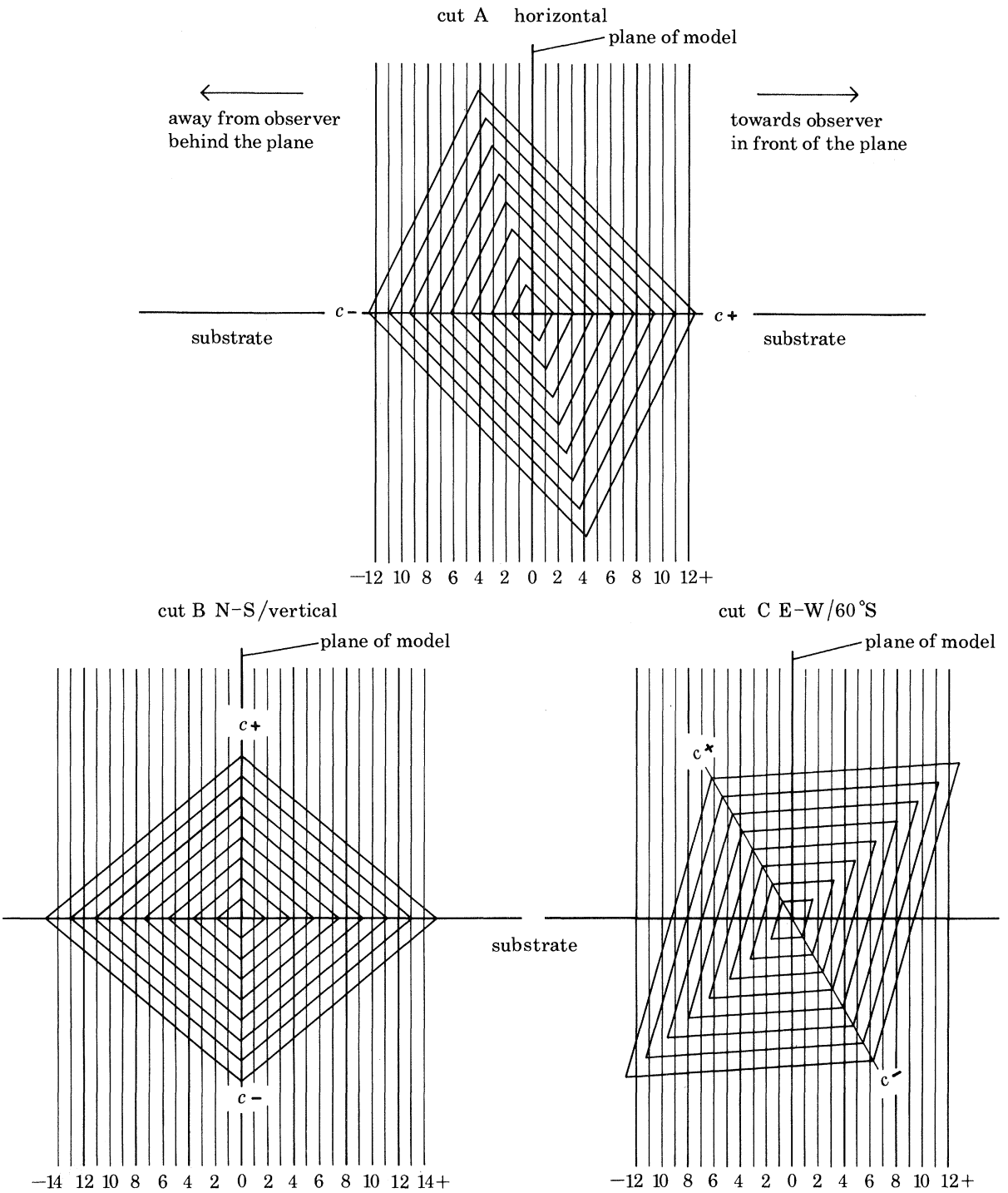

FIGURE 8. Diagrams to show the relation between substrate, plane of crystal growth diagram or model plane, and the planes of crystal cutting through a $\{10\bar{1}1\}$ rhombohedron. Observer views planes end-on (from left of figure 7) so the substrate appears as a horizontal line at eye level. The three directions of cutting are shown separately, in each case the rhombohedron has its centre where the crystal growth diagram plane meets the substrate. The three rhombohedra are sliced normally to the A, B and C cuts to show the position of eight growth zones in the three diagrams. The planes of crystal cutting are numbered at the base of each diagram. The position of these planes corresponds to the rows of nuclei shown in figure 7; nuclei 1 to 5 are sited on the 0 plane which is also the plane of the crystal growth diagram. Planes 0, ±1, ±4, ±8 and ±12 correspond to the templates shown on figures 4 to 6.

of the crystal growth diagram, or model, is vertical. Three $\{10\bar{1}1\}$ rhombohedra are shown with their nuclei on the line of intersection between the substrate and the plane of the model. The rhombohedra show the central templates of the A, B and C cuts coincident with the plane of the model. All templates in figure 8 have their unique orientation directions normal to the substrate in the model plane (or in the 360°/000° direction).

In figure 8, cut A, the rhombohedron is positioned with its *c*-axis in the plane of the substrate, so the A templates are parallel to the plane of the model. The vertical lines passing through the crystal represent a series of A cuts or templates seen end-on; the heavy lines (numbered -12, -8, -4, 0, $+4$, $+8$ and $+12$) represent the templates shown on figure 4 row A. A crystal nucleating on the substrate where the line $+4$ meets the substrate will produce a zonal pattern on the model plane, which will correspond to the template produced by the cut -4. Conversely, if nucleation occurs where a negative line intersects the substrate, its zonal pattern on the model plane is given by a template with a corresponding positive number.

A line from the centre of a crystal drawn normally to the templates lies in the plane of the substrate (figure 8). This line intersects each template at a point that is used to position the template, when constructing the crystal growth diagram. Such a line passes through the centre of every A and B template where the zones are symmetrically arranged around the point. In the case of the C templates, the zonal pattern is not symmetrically arranged around these points (figure 8, planes C; figure 4, column C).

(*e*) *Construction of crystal growth diagrams*

Initially, a horizontal, straight base-line is constructed, which is the line of intersection between two planes, the substrate and the plane of the crystal growth diagram. Five nuclei occur on this line (figure 7), and the positions of the remaining 146 nuclei are projected (normally) on to this base line. All crystals commence growth simultaneously. All templates that include the first growth zone, which will be those belonging to nuclei on or close to the base-line, are plotted. The portion of zone one that extends furthest from the base-line belongs to that crystal which occupied the space first. That is, it has the fastest rate of growth, and all zones closer to the base-line are ignored. Each consecutive zone is considered in turn until the required number of zones is constructed. When 2 or more growth zones are plotted, the position of the intercrystalline boundaries are marked where the same growth zones for adjacent crystals intersect. In practice, all 151 templates need not be considered simultaneously. Templates belonging to crystals nucleated away from the base-line do not contain the early zone lines: they expend their early zones growing towards the plane of slice. During later growth, when growth zones well away from the base line are being considered, many crystals that possess slow growth rates relative to other crystals have become eliminated by the faster-growing crystals. However, even with this reduction in number, it is impossible to show the construction lines used to produce the crystal growth diagrams. The crystal growth diagrams presented here have been terminated away from the base-line before the stage where all crystal's are extending normally from the base-line at the same rate (Grigor'ev's parallel/columnar stage, 1965).

The 151 crystals considered in the three models interact once growth starts, as they compete for space. This interaction is modified at the margins of the diagrams because of edge-effects. These are particularly pronounced along the right and left margins of the diagrams, for the nuclear grid (figure 7) terminates abruptly. Hence, the centre of the diagrams presents a more realistic image. Another edge-effect must be considered, that caused by the termination of

PHILOSOPHICAL TRANSACTIONS OF THE ROYAL SOCIETY A MATHEMATICAL, PHYSICAL & ENGINEERING SCIENCES

nuclei at rows 132–151, and 140–147. Crystals nucleated beyond these rows can grow over intervening crystals to reach the plane of the model. To achieve this, the crystals would require ideal orientation of their g.g.vs, and then they would appear in the crystal growth diagram well above the base line. Examination of figure 13 shows that a crystal developed from nucleus 142 of the outer row does impinge in the diagram. However, with increasing distance of the nucleation point from the base-line, the probability that a developing crystal will reach the plane of the diagram is reduced.

4. Significance of the new diagrams

(*a*) *Initiation of crystals*

Crystal growth diagrams by previous workers all show every component crystal both originating on the base-line, and making just one appearance in the diagram, because only nucleation points on the base-line are considered. Figures 9, 10 and 11 show many crystals commencing above the base-line in the plane of the diagram. These crystals develop from nuclei sited on the substrate either in front or behind the plane of the diagram and have grown into that plane. Individual crystals may pass in and out of the plane several times producing multiple appearances in the diagram. Sometimes several isolated patches belong to the same crystal, for example, in the right-hand centre of figure 12, the two similarly oriented slivers of crystal 81 match well with each other. Conversely, in figure 13, crystal 24 makes four apparently unrelated appearances. These multiple appearances are, of course, connected in three dimensions.

(*b*) *Crystal shape*

The development of preferred shape (long axis) orientation normal to the substrate, an increase in crystal size with a concomitant decrease in crystal number away from the substrate, are features shown in all crystal growth diagrams. These features are corroborated in figures 12, 13 and 14.

Kendall & Broughton (1978) noted several features of para-axial cements (space-filling polycrystalline aggregates crystallized from a substrate, which are directly analogous to the crystal growth diagrams) that are relevant here. In discussing the factors which control the angular relationships of intercrystalline boundaries, they note that similarly oriented (presumably optical or *c*-axis orientation), or equally favourably oriented crystals (presumably in terms of growth rate), have their boundaries approaching a position normal to the substrate. Favourably oriented crystals, they stress, continuously and uniformly expand at the expense of less favoured or slower growing crystals away from the substrate. Kendall & Broughton (1978) in common with Bathurst (1971), Bricker (1971), and others, state that boundaries are commonly planar, and Kendall & Broughton (1978) pointed out they do not display irregular re-entrants. These features may be demonstrated on early crystal growth diagrams, but examination of figures 9–14 show how these earlier diagrams can be misleading.

The orientation of crystal boundaries is not simply related to crystallographic orientation or

---

Figures 9, 10 and 11. Crystal growth diagrams produced from different templates and the nuclei arrangement shown in figure 7. Templates used: figure 9, $\{10\bar{1}1\}$; figure 10, $\{40\bar{4}1\}$; figure 11, $\{01\bar{1}2\}$. Intercrystalline boundaries are shown in heavy lines; crystal zones in light lines.

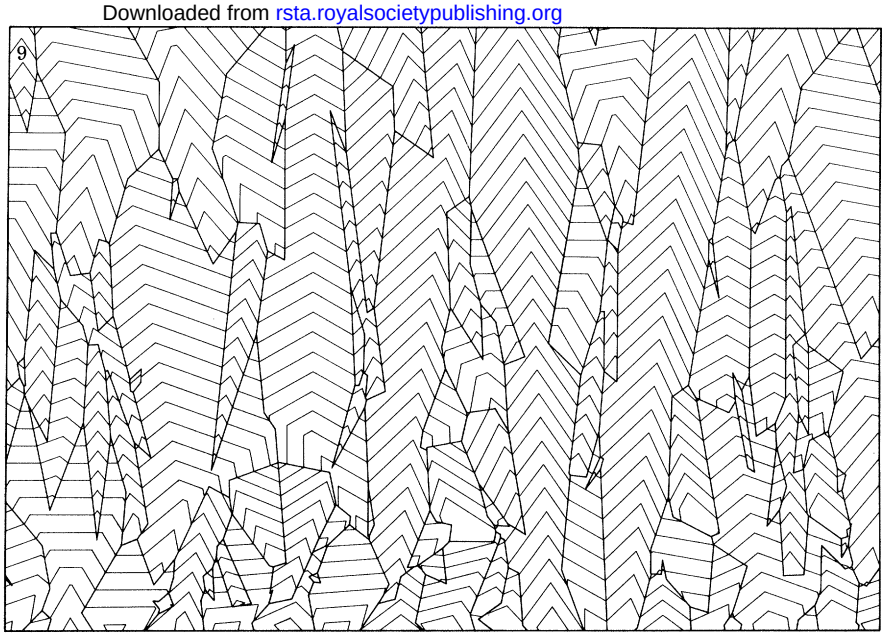

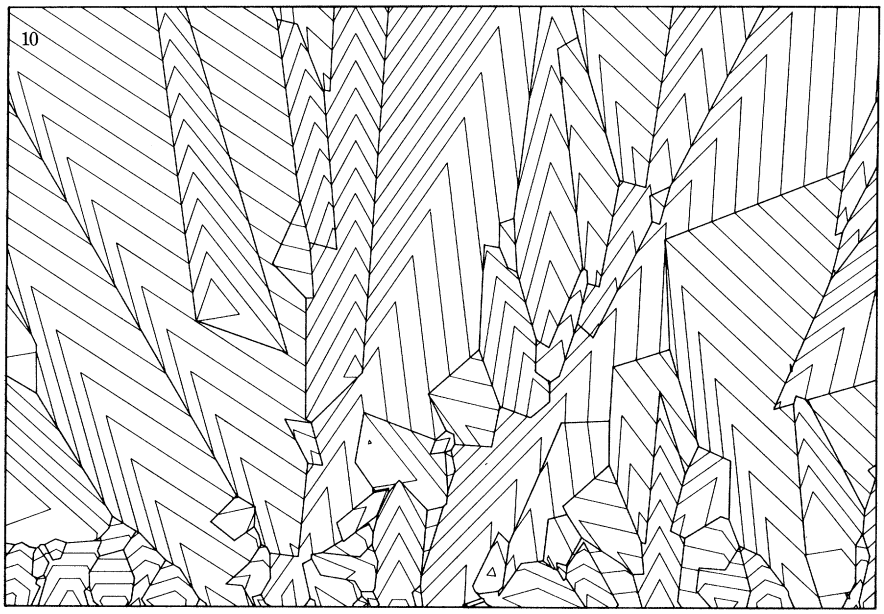

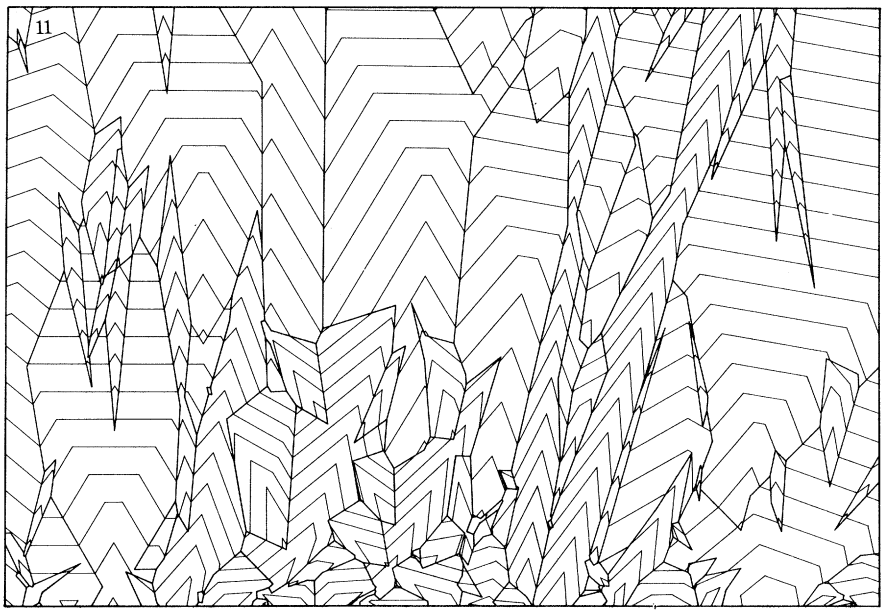

FIGURES 9, 10 AND 11. For description, see opposite.

PHILOSOPHICAL TRANSACTIONS OF THE ROYAL SOCIETY A MATHEMATICAL, PHYSICAL & ENGINEERING SCIENCES

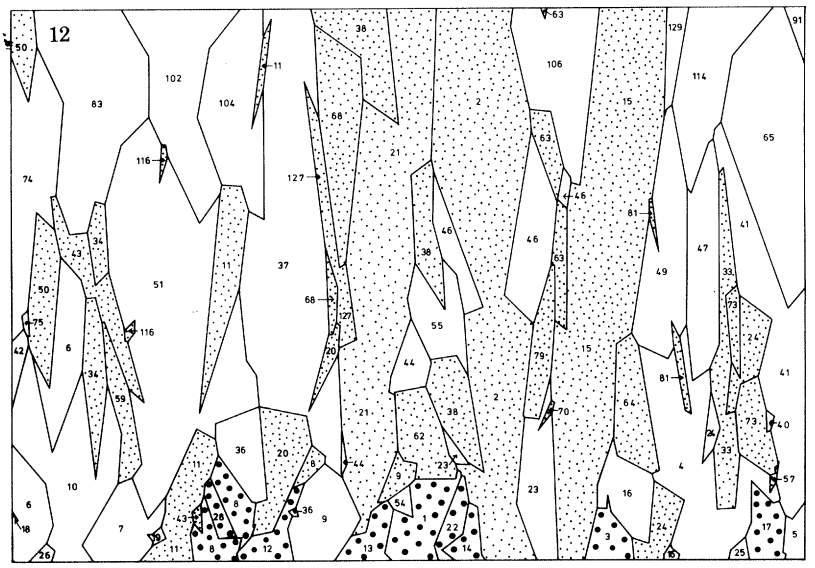

FIGURE 12. Crystal growth diagram produced from {10$\bar{1}$1} templates; complement of figure 9. Intercrystalline boundaries are shown and each crystal is numbered according to its nucleus position on the substrate, as shown in figure 7. Crystals that possess an elongate shape and have their *c*-axes both close to the plane of the diagram and normal to the long axis of the crystal are shaded with light stipple. Crystals which possess an elongate shape and have their *c*-axes both close to the plane of the diagram and parallel to the long axis are shaded with heavy stipple. Unstippled crystals are basal sections (A cuts), possess equant shape in two-dimensions, or the *c*-axis is not clearly normal or parallel to the long axis.

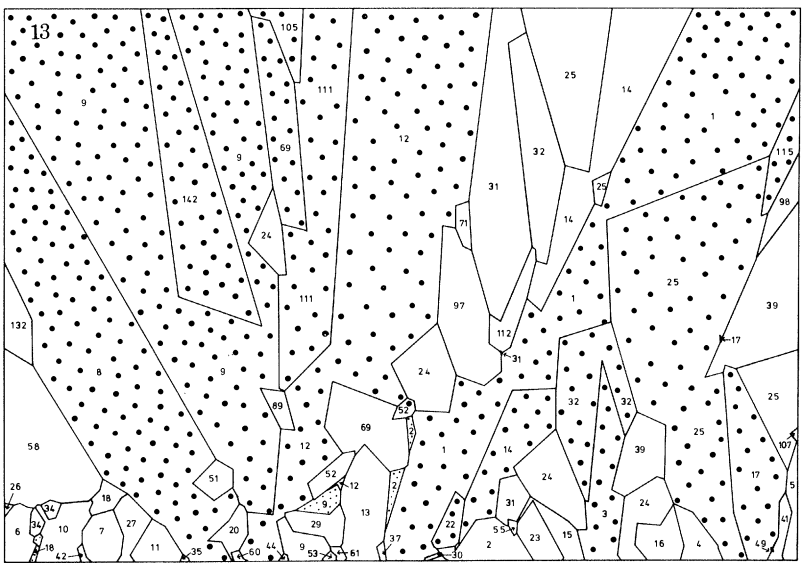

FIGURE 13. Crystal growth diagram produced from {40$\bar{4}$1} templates; complement of figure 10.

the g.g.vs of impinging crystals in the *two dimensions* of crystal growth diagrams. It is the orientation of crystal faces and all growth vectors in the plane of the diagram that control the positions of intercrystalline boundaries. The position of the optic or *c*-axis, and the g.g.vs, may bear no relation to orientation of intercrystalline boundaries. To illustrate this point, examine crystals 9 and 142, left top of figure 13, where crystal 142 is surrounded by crystal 9 in the plane of the diagram. Crystals 9 and 142 show constant orientation of their *c*-axes or g.g.vs, which are

coincident in $\{40\bar{4}1\}$ rhombohedra. However, there are three intercrystalline boundaries of widely differing orientation between these two crystals and, hence, the position of these boundaries cannot be uniquely related to their optic axes, or their most rapid growth directions. The development of the three intercrystalline boundaries between crystals 9 and 142 is shown in figure 10, where the three differently oriented faces of crystal 142 each make their own boundary with the one constantly oriented face of crystal 9.

The change from protomorph to mesomorph, or mesomorph to holomorph (and so on), causes a change in the number and orientation of crystal faces in the templates used to produce a crystal growth diagram. Such a change in template form will be reflected by a complementary change in the orientation of an intercrystalline boundary, without any change in optical orientation or position of the g.g.vs of adjacent crystals.

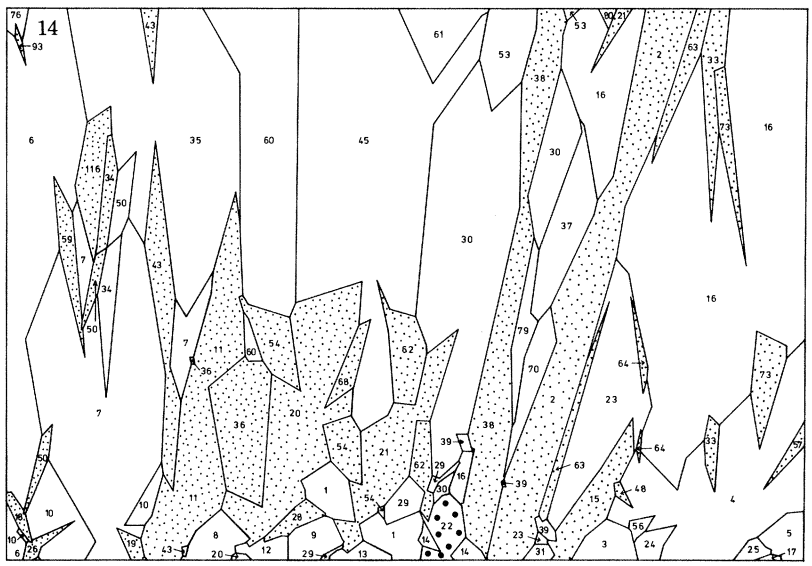

FIGURE 14. Crystal growth diagram produced from $\{01\bar{1}2\}$ templates; complement of figure 11.
For figures 13 and 14, intercrystalline boundaries are shown and each crystal is numbered according to its nucleus position on the substrate, as shown in figure 7. Ornament as in figure 12.

The most favourably oriented crystals in a crystal growth diagram do not continuously and uniformly expand in the plane of the diagram. For example, crystal 31, lower right centre of figure 13. Template 31 contains a g.g.v. oriented normally to the substrate (the most favourable position), but it is soon eliminated from the plane of the diagram. It must, however, continue its growth away from the plane of the diagram to reappear in the centre of figure 13 (arrowed) and again towards the top of the diagram. At the top of the diagram, crystal 31 is being encroached upon by crystals 12 and 25, but it must eventually grow beyond these crystals because of its more favoured orientation. Clearly this crystal and others in figure 12 and 14 possess favourably oriented g.g.vs but do not continuously and uniformly expand at the expense of their neighbours.

The impression gained from early crystal growth diagrams is that component crystals are of simple polygonal shape, but figures 12, 13 and 14 show that the crystals are often extremely irregular in shape, with sharp re-entrant boundaries. For example, crystal 32, lower right figure 13.

PHILOSOPHICAL TRANSACTIONS OF THE ROYAL SOCIETY A MATHEMATICAL, PHYSICAL & ENGINEERING SCIENCES

(*c*) *Crystallographic form*

The plan of nuclei shown in figure 7 is used for all three models so the difference in growth pattern between figures 9–11 and 12–14 is caused by crystallographic form alone. In addition, the width of each growth zone (measured normally to the crystal faces) is kept constant, but as each form has a different surface area, the mass added for any particular growth increment varies, being greatest for the $\{40\bar{4}1\}$ form and least for the $\{10\bar{1}1\}$ form. Consequently, fewer growth zones are required to complete figure 10 $\{40\bar{4}1\}$ than figure 9 $\{10\bar{1}1\}$.

The crystal growth diagrams produced from the $\{10\bar{1}1\}$ and $\{01\bar{1}2\}$ forms are similar, but differ from that produced from the $\{40\bar{4}1\}$ form. This is despite the fact that the $\{01\bar{1}2\}$ form is the exception in being a negative rhombohedron, while the $\{10\bar{1}1\}$ and $\{40\bar{4}1\}$ forms are

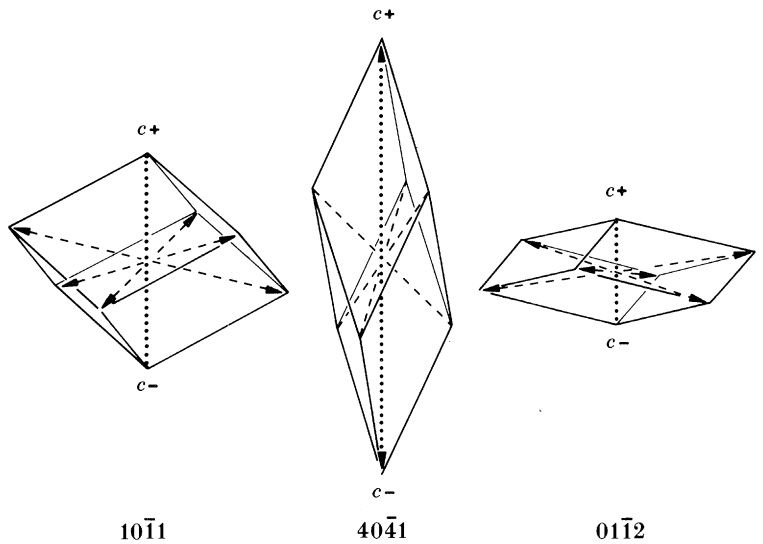

FIGURE 15. $\{10\bar{1}1\}$, $\{40\bar{4}1\}$ and $\{01\bar{1}2\}$ rhombohedra shown in conventional crystallographic position. Relations between *c*-axis and greatest growth vectors (g.g.vs) are shown: ····, growth vector and *c*-axis coincident; – – –, growth vector; , greatest growth vector.

positive. These similarities and differences can be related to the number, position and magnitude of the g.g.vs in the three crystallographic forms (figure 15). The $\{10\bar{1}1\}$ and $\{01\bar{1}2\}$ forms possess six g.g.vs which are oriented at high angles to the *c*-axis, whereas the $\{40\bar{4}1\}$ form has only two g.g.vs which are coincident with the *c*-axis.

The crystal growth diagram (figures 10 and 13) constructed from templates of the $\{40\bar{4}1\}$ rhombohedron include few B templates containing a g.g.v. oriented normally, or near normally, to the substrate. However, these few templates possess great potential to eliminate not only poorly oriented B templates, but also the A and C templates. This potential is high because the magnitude of the g.g.v. in the $\{40\bar{4}1\}$ form, being 4.08, is greater than most other growth vectors (table at base of figure 5). This is in contrast to the situation in the $\{10\bar{1}1\}$ and $\{01\bar{1}2\}$ diagrams where the g.g.vs are 1.97 and 3.04 respectively, values exceeded by several apparent growth vectors.

The A template dominates the distal portions of the $\{10\bar{1}1\}$ and $\{01\bar{1}2\}$ diagrams (figures 9 and 11) while not one A template reaches the top of figure 10 (the $\{40\bar{4}1\}$ diagram). This is because the growth vectors for the A template of the $\{40\bar{4}1\}$ form, 1.03, 1.19 and 2.06

figure 5), are much less than some of the growth vectors contained in the B (g.g.v. = 4.08) and the C (2.23, 3.63, 3.70 and 4.80) templates. The A template of the $\{10\bar{1}1\}$ form possesses a growth vector, 2.85 (figure 4), greater than the g.g.v. = 1.97, and the A template in the $\{01\bar{1}2\}$ form possesses the largest apparent growth vector, 4.57 (figure 6), which also exceeds the g.g.v. = 3.04.

(*d*) *Maturation*

Grigor'ev (1965) pointed out how there is a progression of textural properties as growth proceeds from separate crystals on a substrate, through a drusy stage where the slowly growing crystals are eliminated, to a final stage of constant, parallel-columnar growth. The models presented here (figures 9–14) show Grigor'ev's first stage, most of the second stage and the

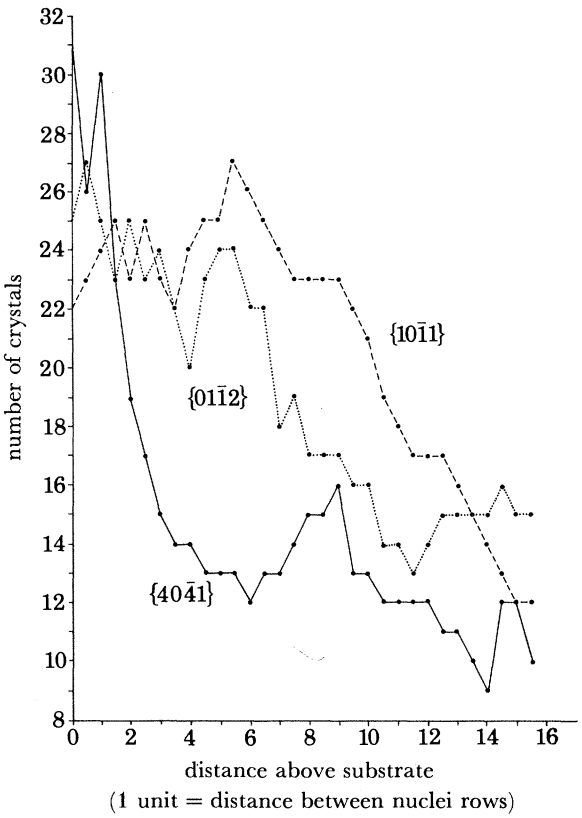

FIGURE 16. Plot showing the reduction in the number of crystals against the distance above the substrate in crystal growth diagrams for the $\{10\bar{1}1\}$, $\{40\bar{4}1\}$ and $\{01\bar{1}2\}$ rhombohedra. The unit of distance measured above the substrate arbitrarily corresponds to the distance between the rows of nuclei on the substrate shown on figure 7. The rapid decrease in crystal numbers shown by the $\{40\bar{4}1\}$ form is contrasted with that from the $\{10\bar{1}1\}$ and $\{01\bar{1}2\}$ forms. Data taken from figures 12, 13 and 14. Further analysis is provided in the text.

transition to the third stage. There is no clear cut dividing line between the three stages; the change from one stage to another is not synchronous. This maturation can be demonstrated simply by the decrease in crystal numbers, distally, away from the substrate. The rate of declining crystal numbers for the three models is shown in figure 16. The rapid fall-off in numbers with the $\{40\bar{4}1\}$ form accords with previous crystal growth diagrams, but the $\{10\bar{1}1\}$ and $\{01\bar{1}2\}$ forms show a plateau region, or initially a rise in crystal numbers, away from the substrate. This difference in behaviour is due to a narrower range in magnitude, and a more even spread of growth vectors, between the A, B and C templates in the $\{10\bar{1}1\}$ than is present

in the {40$\bar{4}$1} templates. The less ruthless elimination of crystals with {10$\bar{1}$1} and {01$\bar{1}$2} growth allows a greater number of crystals, seeded adjacent to the plane of the diagram, to reach into that plane. This region, where as many crystals are eliminated as new ones are introduced, can be regarded as an additional stage of aggregate crystal growth, which is only present when certain crystallographic forms are considered.

The pattern of a crystal growth diagram can be assessed if the component crystals are closed crystallographic forms and their growth vectors are known. An equant, closed crystallographic form with many faces, being close to a sphere, where all true growth vectors are equal, will

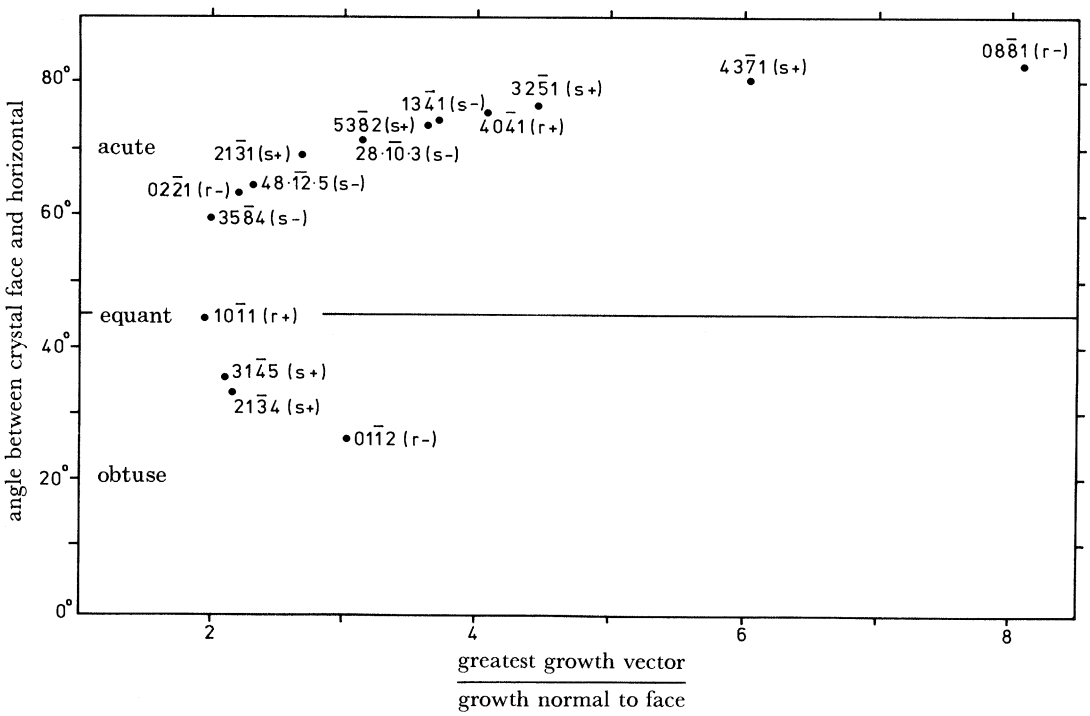

FIGURE 17. Plot of angular relations of calcite crystal faces against the ratio of the largest to the smallest growth vectors for closed crystallographic forms. Angular data from Palache *et al.* (1951). The general shape of the entire crystallographic form is indicated as acute, equant or obtuse. Scalenohedra and rhombohedra are indicated s and r respectively, while positive and negative forms are + or −.

display the slowest textural maturation. The change in the numbers of crystals away from the substrate may increase initially, then remain constant before declining slowly; as seen in figure 16 for the {10$\bar{1}$1} form. Acute rhombohedra such as the {40$\bar{4}$1} form are elongate in one direction; along the *c*-axis. As the angle between the crystal face and the horizontal increases, so the form becomes more elongated, and the magnitude of the g.g.v. increases relative to growth measured normal to a face. In elongate forms there is a rapid textural maturation and decrease in crystal numbers away from the substrate. The rate of diminution in crystal numbers shown for the {40$\bar{4}$1} form (figure 16) would be eclipsed if the {80$\bar{8}$1} were used, for its g.g.v. is almost double the magnitude of the {40$\bar{4}$1} g.g.v. Figure 17 shows the relationship between the magnitude of the g.g.v. and the crystal face angles of 15 documented rhombohedra and scalenohedra (Palache *et al.* 1951).

Obtuse rhombohedra are somewhat disc-shaped, in a manner of speaking. They are drawn

out in a plane rather than along a line as in the acute forms. This is reflected in the obtuse rhombohedra possessing six rather than two g.g.vs. In obtuse forms, there is a greater chance that a random cut will intersect, or pass close to, a g.g.v., than in an acute form. Therefore, the rate of decline in crystal numbers away from the substrate will be less for an obtuse rhombohedron than for an acute rhombohedron with the same magnitude of g.g.vs. In obtuse forms, as with acute forms, an increased rate of diminution in crystal numbers away from the substrate occurs with increasing magnitude of the g.g.v.

The discoidal shape of obtuse rhombohedra causes crystals in the mature stage of aggregate growth to develop a bladed or tabular shape. This feature is emphasized in figure 14, where a mixture of narrow and broad crystals is present. The narrow crystals have their *c*-axes parallel both to the surface of the diagram, and to the base-line (B templates; for example crystals 38, 43, 2, 63 and so on, from figure 14). The broad crystals have their *c*-axes oriented normally to the surface of the diagram (A templates; for example crystals 6, 35, 60, 45 and so on, from figure 14). This division into narrow and broad crystals is artificial; crystals of intermediate width can be produced by considering other cuts through the $\{01\bar{1}2\}$ crystal. However, the wide range of crystal widths distinguishes obtuse from acute or equant crystal growth, a distinction more readily made by examination of a crystal growth diagram oriented parallel to the substrate. The bladed or tabular shape developed from obtuse forms in the final stage of maturation renders Grigor'ev's term 'parallel-*columnar*' stage something of a misnomer.

The textural features shown by crystal growth diagrams can be predicted if the crystallographic form of the crystals is known. The three basic shapes $\{10\bar{1}1\}$, $\{40\bar{4}1\}$ and $\{01\bar{1}2\}$ modelled here can be applied to other closed crystallographic forms. The most distinctive crystal growth diagrams are produced from rod or spindle-shaped crystals with extreme length to width ratios, and blade-shaped crystals with extreme length to width and breadth ratios. As the dimensions of rod and blade-shaped crystals approach the equant shape, so there is a convergence in the properties of their derived crystal growth diagrams. However, in the final stage of maturation in a crystal growth diagram, there remains one property which can be used to distinguish acute (rod) from obtuse (blade) parentage: optical elongation.

(*e*) *Elongation*

Crystals with extreme length to width ratios develop if the final mature stage of impingement growth is prolonged. The elongate shape of such crystals is due to parallel alignment of their g.g.vs and intercrystalline boundaries normal to the substrate. Lindholm (1974) has correlated crystallographic habit with morphology; the length to width ratio in pore-filling calcites from septarian veins. However, the length to width ratio of crystals, as measured in thin section, is unrelated to crystallographic form or habit. Elongate crystals will develop during the mature stage of impingement growth irrespective of the crystallographic form involved.

Acute crystallographic forms have their two g.g.vs coincident with the *c*-axis (figure 15) so, during mature elongate growth, their *c*-axes are also oriented normally to the substrate. The coincidence of the crystal's long axes and *c*-axes renders the fast-ray vibration direction parallel to the optic axis, and hence the crystals are length-fast or exhibit negative elongation.

Obtuse crystals are more complex, for their g.g.vs are oriented at a high angle to the *c*-axis and consequently they are approximately length-slow (Dickson 1978). The angular relations between the g.g.vs and *c*-axes of four calcite forms are shown in figure 18. The $\{21\bar{3}4\}$

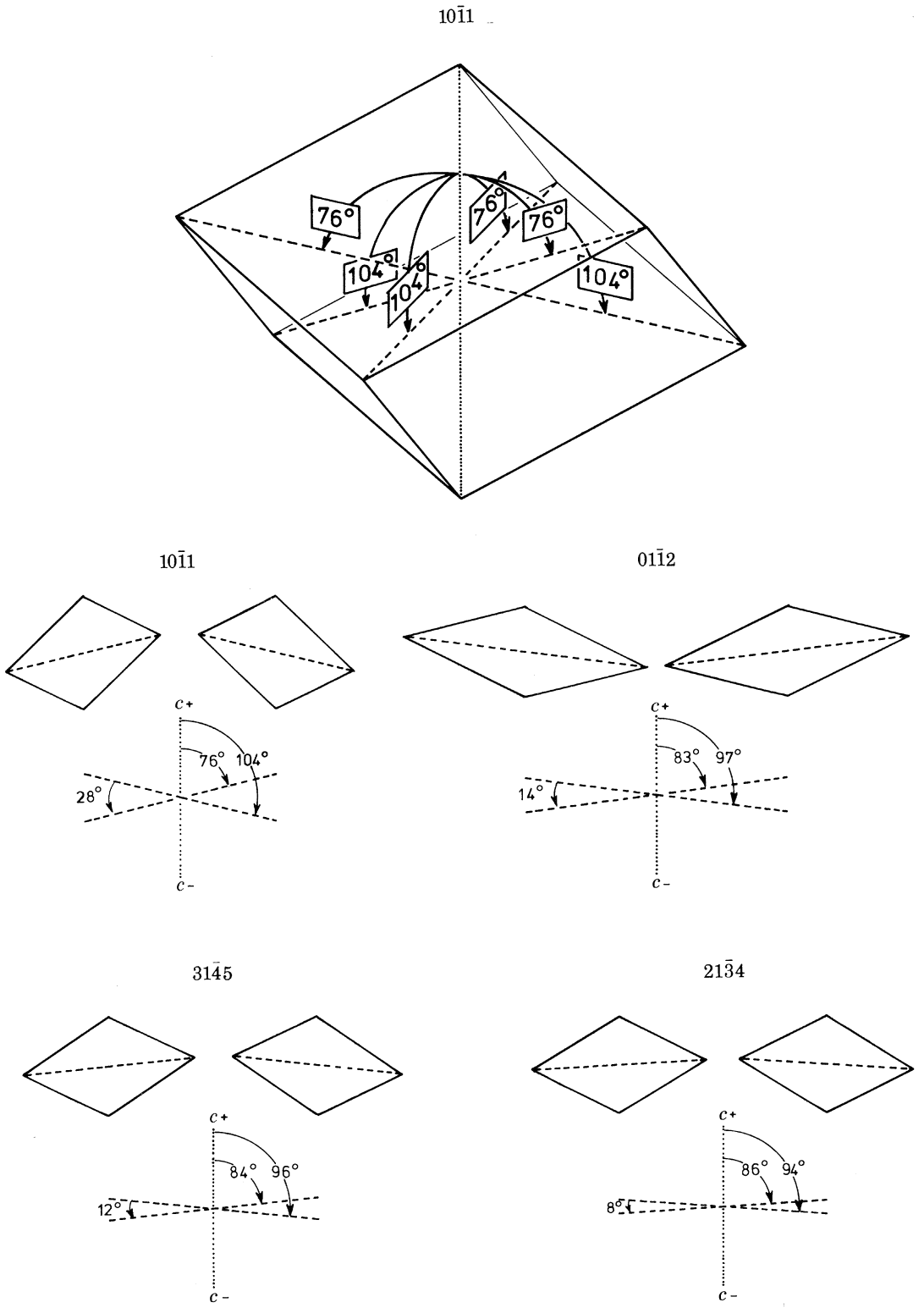

FIGURE 18. *Top*: Perspective view of {10$\bar{1}$1} rhombohedron showing positions of six g.g.vs and their angular relations to the *c*-axis. In *lower four diagrams* each group shows two slices which include two g.g.vs and the *c*-axis and the angular relations between the g.g.vs and the *c*-axis for four, common, closed, calcite crystallographic forms.

scalenohedron (figure 18), if developed into elongate crystals, will be the nearest to being truly length-slow, for the angles between the g.g.vs and the *c*-axis (86°/94°) are closest to 90°. Folk & Assereto (1976) in describing 'tooth-shaped packets of length-slow calcite from speleothem deposits from Carlsbad Caverns', noted that the crystals are elongate, either perpendicular, or at an angle of 60°, to the *c*-axis. They ascribe the 60° orientation to crystal development parallel to a (unit) rhomb face. However, most of this angular discrepancy can be accounted for in another way. The angle between the g.g.v. and *c*-axis (in a slice containing both) for a $\{10\bar{1}1\}$ rhombohedron is 76°. All crystals in a slice through a mature $\{10\bar{1}1\}$ aggregate, will contain a g.g.v. normal to the substrate, but only some will contain the *c*-axis and yield an angle of 76°. These cuts, which do not contain the *c*-axis, will show greater apparent angles until the *c*-axis is oriented normally to the slice when the *c*-axis and the g.g.v. will apparently be coincident. Hence, the angle between the long axis of the crystal (equivalent to g.g.v.) and the *c*-axis of the crystals in a $\{10\bar{1}1\}$ aggregate should vary between 76° and 90° in a two dimensional slice. The approximately length-slow calcite developed from all obtuse rhombohedra and scalenohedra will consequently display oblique extinction.

A mature aggregate developed from an obtuse form may also be distinguished from that developed from an acute form by differences in the relief displayed by the component crystals. Acute, mature crystals possess uniform relief. As the g.g.vs and *c*-axes are coincident, they will both intersect any slice with an identical orientation. The g.g.vs in a mature aggregate developed from obtuse crystals must also intersect any slice with an identical orientation, but the *c*-axis may intersect the slice at a variable angle. The difference in relief of two adjacent crystals in an obtuse aggregate will be greatest where one crystal includes its *c*-axis in the plane of slice and the adjacent crystal has its *c*-axis normal to the plane of slice. This difference in relief will be greatest for the crystallographic form which possesses an angular difference between the g.g.vs and the *c*-axis closest to 90° (no closed form exists where this angle is 90°). This character is very distinctive for trigonal carbonates because of their particularly high birefringence.

A further distinguishing feature between mature aggregates developed from obtuse, as opposed to acute, rhombohedra is the crystal shape. The mature portion of figure 14 (obtuse) shows the crystals to be of both wide and narrow shape, while in figure 13 (acute) such a distinction cannot be made. The $\{01\bar{1}2\}$ rhomb is flattened along its *c*-axis, and in the mature stage of growth the crystal is on its side with one g.g.v. normal to the substrate. In such a position, the flattened shape of the $\{01\bar{1}2\}$ rhomb produces tabular or bladed crystals. In contrast, the spindle-shaped $\{40\bar{4}1\}$ rhomb produces columnar crystals. This feature is over-emphasized in figures 13 and 14 because only three directions of crystal cutting are considered.

Figures 10 and 13 show maturation to predominantly length-fast (coarse stipple; B and some C templates) crystals which have parallel extinction and uniform relief. Figures 11 and 14 show maturation to a more complex arrangement of wide basal (A templates, unornamented) sections and strongly elongate, narrow length-slow (fine stipple; B and some C templates) sections of contrasting relief and oblique extinction.

(*f*) *Triple junctions*

A triple junction is the point at which three intercrystalline boundaries meet. A voluminous literature exists on triple junctions where there is a tendency to develop $3 \times 120°$ angles by the migration of intercrystalline boundaries as they approach lower energy levels. However, the intercrystalline boundaries discussed here are of the impingement and not the adjustment type.

Once formed, an impingement boundary is static; if it moves, it is no longer of the impingement type.

Bathurst (1964) described a special type of triple junction in which one angle measured 180°. This type of triple junction he termed enfacial. He argued that the 180° angle is unlikely to arise during synchronous growth of three crystals for this would involve the unlikely coincidence of either two intercrystalline boundaries, or an intercrystalline boundary and a crystal face, developing as a single continuous plane. However, figure 19 shows two examples of enfacial junctions produced from three synchronously growing crystals. The situations shown here, where two crystals progress by single faces and their mutual boundary is met by a third crystal

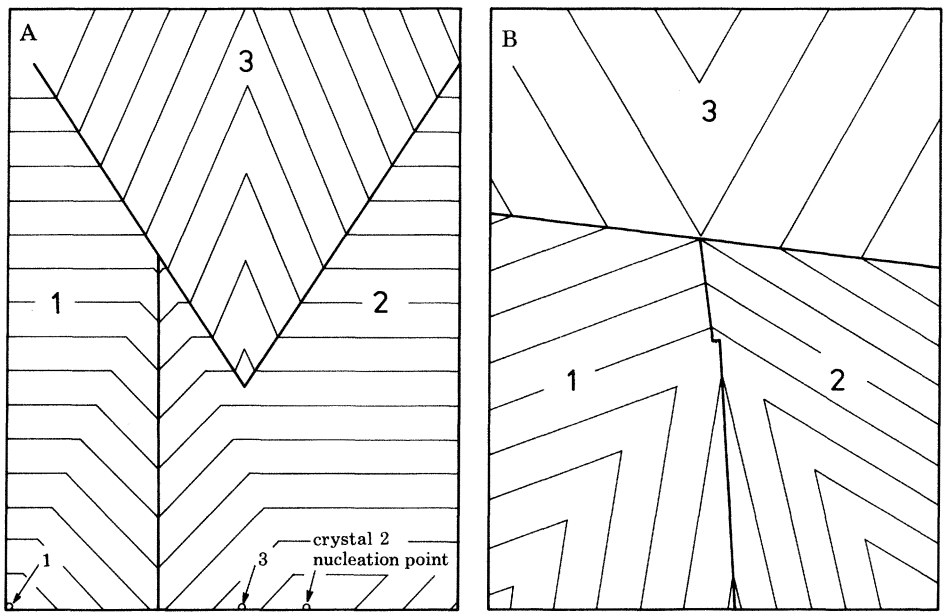

FIGURE 19. Crystal growth diagrams of enfacial junctions. A. This shows how an enfacial junction may appear when crystal 3, seeded on the substrate away from the plane of the diagram, grows into the plane of the diagram interrupting the growth of crystals 1 and 2. Crystals 1 and 2 are both seeded on the baseline of the diagram but are overtaken by crystal 3 because its g.g.v. is more favourably oriented. B. Crystals 1 and 2 approach the enfacial 'point' as single faces while crystal 3 approaches as 2 faces; the apex of the double faced crystal 3 precisely meeting the enfacial point. In situation A or B the planes that form the intercrystalline boundaries between the three impinging crystals meet in a line. There is only one point on this line where a slice of a particular orientation will produce an enfacial junction.

propagated as two faces, must be rare because the slice required to produce an enfacial junction must pass through the line of intersection of the three crystals at the point where the double-faced crystal crosses that line at the exact angle to form an enfacial junction. This combination of events is unlikely to occur frequently.

Enfacial junctions arise, Bathurst (1964) maintained, because the crystal face of one of the three crystals remains stationary, while the other two grow against it. This requires a spasmodic or interrupted growth which is not portrayed in the crystal growth diagrams considered here. Consequently enfacial junctions are not to be expected in these crystal growth diagrams.

The angular relationships of triple junctions is shown in figure 20, (top left) where the largest angle is plotted against the intermediate angle; the smallest angle may be determined by subtracting the sum of the plotted angles from 360°. All triple junctions, except those with one

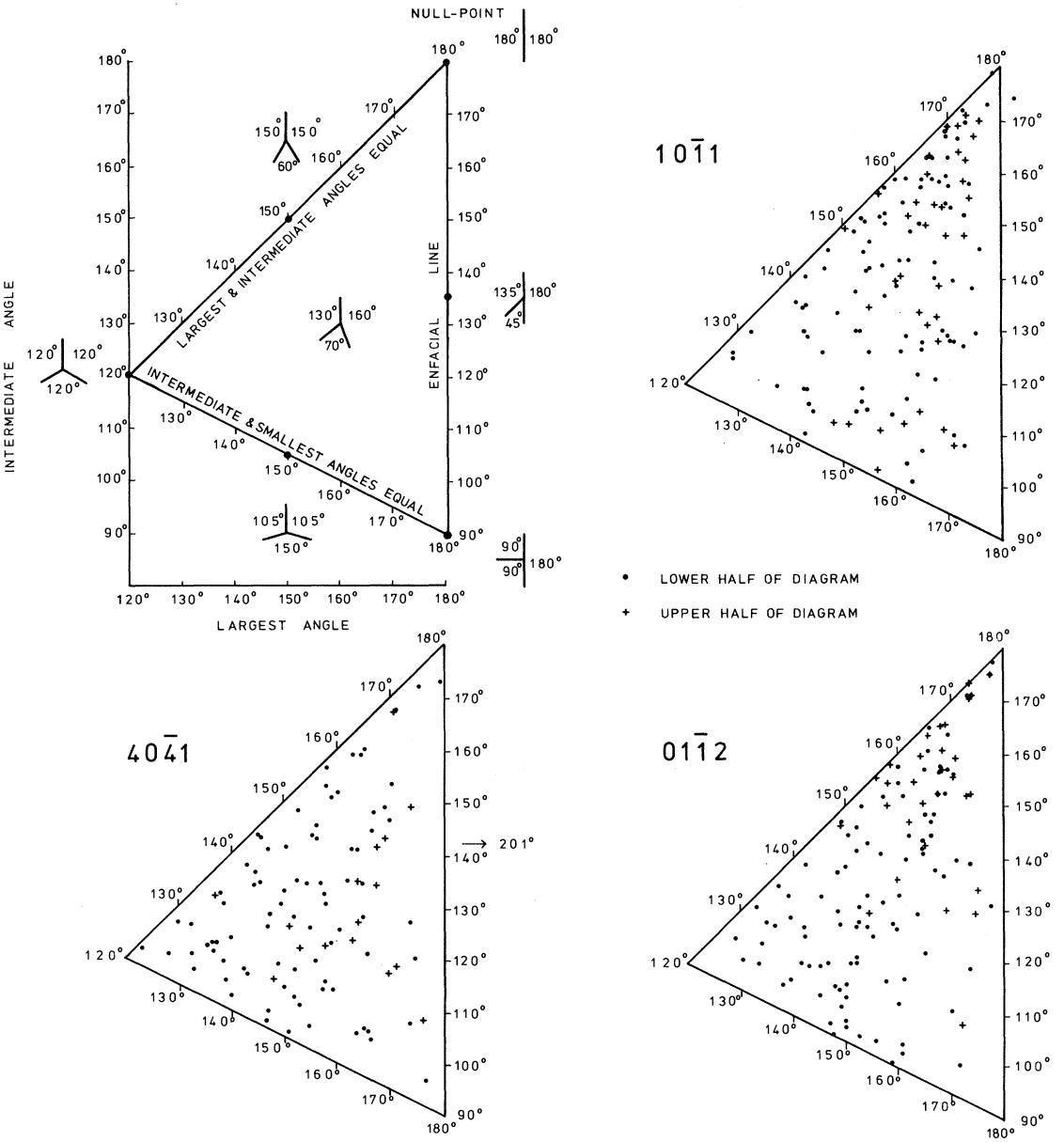

FIGURE 20. Plots showing the angular relations of triple junctions. The intermediate angle is plotted against the largest angle; the sum of these subtracted from 360° gives the smallest angle. *Top left*: diagram showing the triangular area where triple junctions plot when no angle exceeds 180°. Sketches showing triple junctions help to visualise the plotted data. *Top right*: {10$\bar{1}$1} data from figure 9 plotted on a triangular diagram. *Lower left*: {40$\bar{4}$1} data from figure 10 plotted on a triangular diagram. One triple junction with angles of 201°, 142° and 17° is indicated by an arrow. *Lower right*: {01$\bar{1}$2} data from figure 11 plotted on a triangular diagram. Data from figures 9, 10 and 11 are divided into two halves, proximal to the substrate shown as · and the other distal to the substrate shown as +.

angle greater than 180° (two in the 386 measured from figures 12, 13 and 14), plot in a triangular area. In order to compare triple junctions close to the substrate with those away from the substrate, figures 12, 13 and 14 were divided in half by a line parallel to the substrate. The data collected from the proximal area are spread over the entire triangular areas of figure 20 (shown as dots), whereas data from the distal areas (shown as crosses) are noticeably absent

from the $3 \times 120°$ corners. This is due to the increasingly elongate crystal shape in the distal areas. It is worth emphasizing that not one of the 386 triple junctions measured is enfacial.

5. Limitations of the crystal growth diagrams

The development of polycrystalline aggregates by impingement growth from a substrate is influenced by many factors which may be divided into two categories: those relating to the crystals, and those relating to the substrate. In figures 9–14, most of these factors are kept constant so that the effects of differing crystallographic form is demonstrated.

(*a*) *Crystal constraints*

(1) The templates used to produce the crystal growth diagrams were derived from three directions of crystal cutting; two of which (cuts A and B) include several elements of crystal symmetry. The three directions chosen are approximately orthogonal, so the principal variations in the crystal's shape are shown. It is predicted that a greater variety in the direction of crystal cutting, with the introduction of less symmetrical templates, would modify the aggregates pattern only slightly, producing no significant change in its overall development.

(2) A simple, closed crystallographic form is used throughout each of the three crystal growth diagrams. In nature the crystallographic form commonly remains constant spatially, but often changes temporally. This type of change during growth could bring about a dramatic change in the form of the crystal aggregate. For instance, if obtuse rhombohedra were to overgrow acute rhombohedra the status of the g.g.vs would change completely.

(3) The growth zones of every crystal in each of the three rhombohedra considered have a constant width. The use of an open crystallographic form in the basic crystal unit used to produce the templates would necessarily involve at least one other form. A crystal unit composed of two or more forms introduces the possibility of changes in relative growth rates between forms. This would produce a change in the magnitude and probably the orientation and number of g.g.vs, which in turn will affect the form of the crystal aggregate. Varying growth rates which affect different crystallographic forms may produce curved intercrystalline boundaries. Grigor'ev (1965, figure 55) illustrated curved intercrystalline impingement boundaries between two different, but simultaneously growing minerals.

(4) A feature which links the two categories of constraints is the pattern of nucleation. The regular grid system for nuclei positioning used here to expedite construction (figure 7) could be more realistically substituted by a random pattern. However, no significant difference in the crystal growth diagrams would be predicted if such a change were made.

(*b*) *Substrate constraints*

(1) The shape of the substrate has an important effect on growth. Plane substrates, such as those used in this work, may be exemplified by the essentially parallel walls of certain types of vein. Convex substrates give rise to divergent, radiating crystal aggregates while concave substrates give rise to convergent, radiating aggregates. Curved substrates will affect the rate of crystal number decrease away from the substrate (figure 16). Strongly curved substrates are characteristic of enclosed cavities such as vugs or the pores within a sediment.

(2) The substrate in all discussions so far has been passive: each new crystal develops according to the orientation of its nucleus and the impingement of surrounding crystals. However,

PHILOSOPHICAL TRANSACTIONS OF THE ROYAL SOCIETY A MATHEMATICAL, PHYSICAL & ENGINEERING SCIENCES

seeding or epitaxial growth may occur where the new crystals continue the structure of crystals making up the substrate. This leads to an entirely new situation where the structural orientation and surface area of the exposed substrate crystals play a major role in controlling the aggregate's form. For instance, if the substrate crystals are all oriented such that their g.g.vs are normal to the substrate, maturation will be immediate. There will be no crowding out or elimination of poorly oriented crystals; Grigor'ev's stage of isolated crystals will pass directly to the fully mature final stage. Intercrystalline boundaries will be normal to the substrate. The variety of features which occur during epitaxial growth is outside the scope of this paper.

6. Relevance of graphical models to cement diagnosis

Cement as defined by Bathurst (1971, p. 416) is composed of passively precipitated, space-filling carbonate crystals that grow attached to a free surface. The all-embracing nature of this definition leads to the inclusion of cement types which formed at widely differing rates in a variety of different environments. For instance, sedimentary calcite cements may crystallize either from solutions which occupy the entire pore system (phreatic) or from a film of solution which clings to the pore walls, the remaining pore space being air-filled (vadose). The type of growth modelled in this paper is clearly inapplicable to the latter situation where cement is patchily distributed and concentrated in the smaller pores (Dunham 1971). In vadose pores, crystals possess curved terminations mimicking the water/air interface (Schroeder 1973). The manner of crystal growth in vadose liquid films is controlled, at least partly, by exogenetic forces, a feature which clearly distinguishes them from phreatic cements. It is therefore not surprising that individual morphological criteria are not ubiquitous to all cement types.

The philosophy of erecting a single list of criteria for the recognition of all cements is too ambitious: too few characters are common to all cements and too many characters exist, such is the great variety of cement types. In practice the first stage of investigation is to identify the morphological type of crystal aggregate. Then, after examination of other properties (suggested by Bathurst 1971, p. 417), the decision may be made as to whether that morphological type is a cement. The status of the five textural features (mentioned previously) from the list of criteria for the recognition of cements is misleading, for none can be held to be ubiquitous for cement and combined they do not identify one morphological type satisfactorily.

The crystal growth diagrams presented here may be used as models for one particular type of impingement growth. Characteristics derived from these diagrams may be used to identify that particular type of growth but do not directly identify that crystal aggregate as cement. It is feasible that if recrystallization or replacement proceeded from an interface through a solid that presented no obstacle to the growth of new crystals, then an impingement texture of the type modelled could be generated. If such a process removed all trace of the precursor, then cementation cannot be texturally distinguished from recrystallization or replacement.

7. Recognition of impingement growth from an inert substrate

The characteristic features of impingement growth developed from an inert substrate may be listed as follows:

(1) crystals increase in size away from substrate.
(2) crystals have preferred shape orientation with long axes normal to substrate.

PHILOSOPHICAL TRANSACTIONS OF THE ROYAL SOCIETY A MATHEMATICAL, PHYSICAL & ENGINEERING SCIENCES

(3) crystals have preferred orientation of greatest growth vector normal to substrate (a character that cannot be directly observed).

(4) acute closed crystallographic forms give rise to length-fast crystals and obtuse forms give rise to length-slow crystals.

These features are most clearly recognized if the aggregate is well matured; at least well into the drusy stage (Grigor'ev 1965). An immature aggregate may show none of the above features. This is often the case with cements where the crystal nuclei are widely separated on the pore walls relative to the available space into which the crystals can grow. Crystals growing from one wall meet crystals growing from other walls before maturation can occur.

The recognition of impingement growth and cements has relied on external features such as size and shape of the component crystals. However, calcite crystals often possess internal chemical zonation which is taken to be a growth zonation (Evamy 1963; Dickson 1965). This zonation is easily displayed either by staining (same references) or by stimulating cathodoluminescence (Sippel & Glover 1965). Growth zonation is a much more powerful tool than shape or size of crystals for deciphering the geometry of crystal aggregates. The efficacy of using zonation in the interpretation of calcite aggregates is illustrated by an example taken from a small patch reef from the Lower Magnesian Limestone of Permian age exposed in a road cutting at Nuthill, near Aberford, Leeds, Yorkshire (Smith 1981).

The rock is a bryozoan biolithite, and contains late calcite spar as is common in the Magnesian Limestone of England. An unusual feature of this rock is the very large area occupied by this late calcite spar because of the irregular, twig-like ramose bryozoans which form a framework in the calcite spar. The bryozoans and their encrustations are composed of dolomite. Each calcite crystal overlies an isopachous dolomite fringe to the pores. It is possible that each calcite is epitaxially contiguous with just one of the tens to hundreds of dolomite crystals, but this relationship was not observed in the material examined and the dolomite substrate is regarded as inert. Another important feature is the presence of air-filled voids in the spar, centrally placed between the bryozoa. These voids when broken open are seen to be lined by crystal faces.

The pattern of intercrystalline boundaries in this late spar is illustrated in figure 21. The crystals display an overall equant shape (such a texture is usually termed granular or blocky). Clearly, if this is an impingement aggregate generated from an inert substrate it cannot be mature, for none of the four features listed above is observed. The immature nature of this aggregate is supported by the small space available for growth compared with the average size of the crystals. When examining figure 21 it is difficult to envisage these crystals centrally placed between the bryozoans having any connection with the substrate. However, the very irregular shape of the bryozoan framework, and the cut-effect of a thin section explains this apparent discrepancy.

The very irregular shape of some intercrystalline boundaries, such as at point A figure 21, owe their extreme irregularity to a low angle of intersection between the boundary and the section surface. It should also be noted in this context that natural crystals sometimes possess irregular, non-planar faces, which (as they impinge during growth) in turn will cause irregular intercrystalline boundaries.

Data on the angular relations of triple junctions from figure 21 are displayed in figure 22. It is extremely difficult to measure some triple junctions accurately, such as triple point B figure 21,

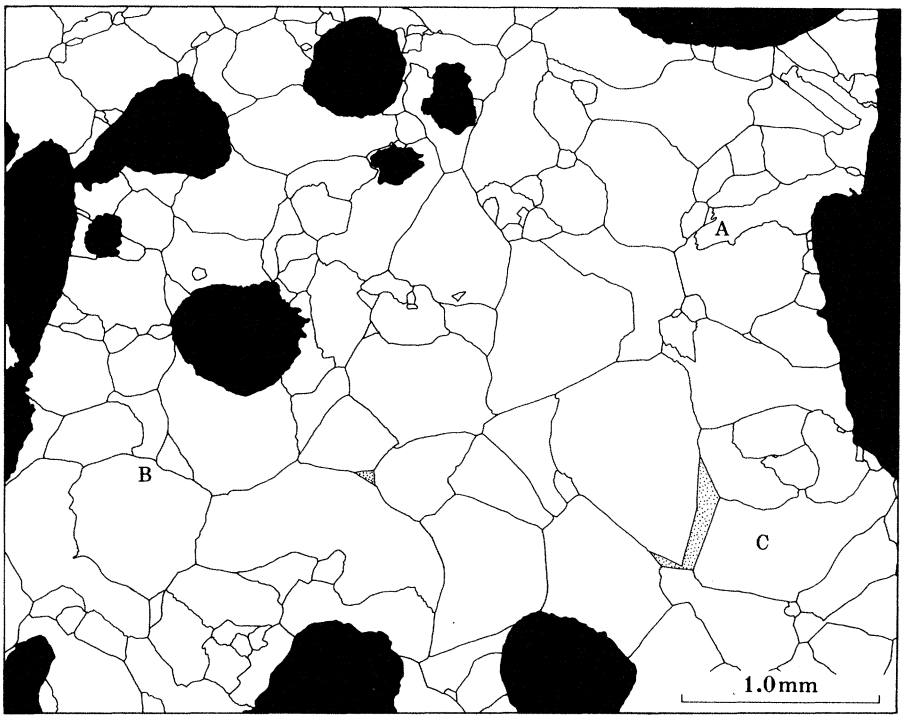

FIGURE 21. Outline from thin section of bryozoan biolithite, from patch reef at Aberford, near Leeds, Yorkshire. Bryozoans, encrustation and isopachous fringe of dolomite are marked in black. The intercrystalline boundaries in calcite spar illustrated almost completely occupy the remaining area, except for two voids shown stippled. A, B and C are referred to in the text.

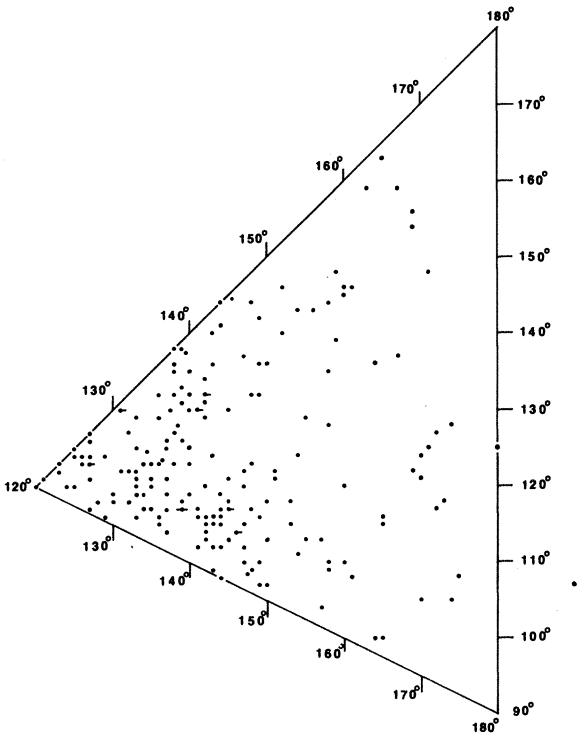

FIGURE 22. Plot showing angular relations of 191 triple junctions measured from figure 21. The construction of the plot is similar to figure 20. Single dot, one triple junction; dot with one bar, two triple junctions; dot with two bars, three triple junctions. Note the similarity between this plot and the data plotted from the proximal crystals (lower half of diagram) in figure 20.

PHILOSOPHICAL TRANSACTIONS OF THE ROYAL SOCIETY A MATHEMATICAL, PHYSICAL & ENGINEERING SCIENCES

but it is clear from figure 22 that there is almost a complete absence of enfacial junctions, as predicted from the crystal growth diagrams.

The origin of the crystal aggregate in this grainstone is inconclusively determined from the information presented in figure 21. Indeed, features present on figure 21 such as curved, somewhat irregular intercrystalline boundaries, and the absence of enfacial junctions have been taken (Bathurst 1971, p. 485 & 490) as indicative of neomorphic spar. However, this spar possesses 14 growth zones, each only a few micrometres in width, which can be displayed by cathodoluminescence. This helps to resolve the problem. The same, or parts of the same, zonal pattern can be recognized in all crystals; hence any point within these crystals can be dated

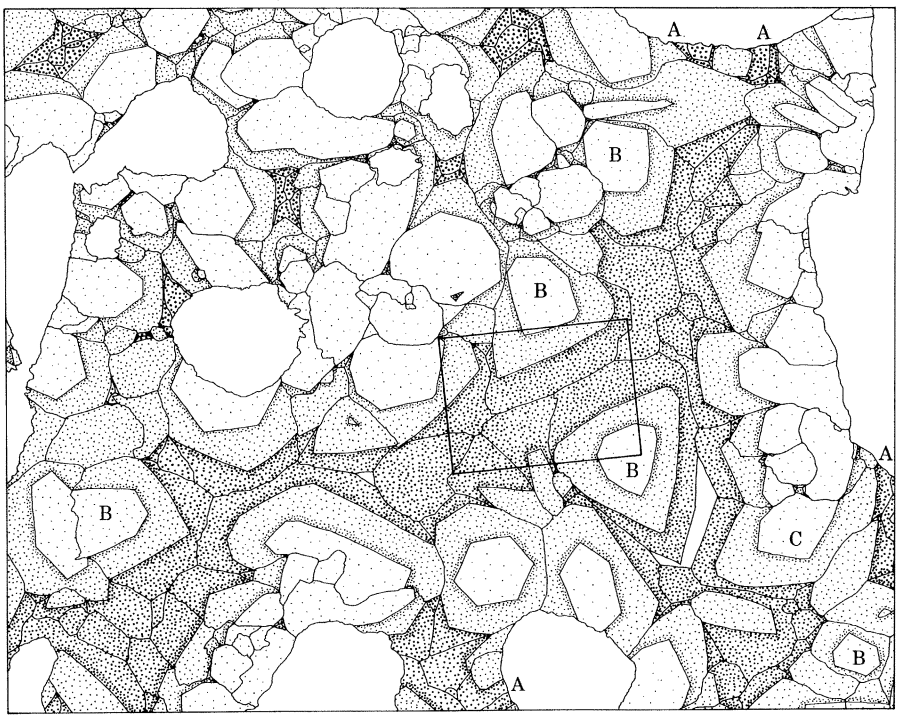

FIGURE 23. Same subject as figure 21. Three areas in calcite crystals divided by two zones: Fine stipple, earliest growth; medium stipple, intermediate age; coarse stipple, latest growth. The two voids are plain. A, B and C are referred to in the text.

relative to the zonation. The position of two zones, which divide the crystals into three equal units, is shown in figure 23. The general distribution of these three units is consistent with impingement growth. The oldest unit occurs predominantly close to the pore walls although considerable scatter does occur. The youngest unit occurs at the centre of the pores culminating in the last cement lining two voids, which escaped complete occlusion. It is apparent from figure 23 that the distribution of nuclei on the substrate was sparse and irregular. Some areas (labelled A, figure 23) were not covered until the last third of crystal growth. This shows the predominantly inert nature of the dolomite substrate which, after the initial nucleation of calcite, was passively overgrown by the spar. Areas of the earliest calcite growth are sometimes positioned well away from the substrate (labelled B, figure 23). The substrate, on which these crystals nucleated, must be close to the plane of the section.

FIGURE 24. Inset area of figure 23. Zones are displayed by cathodoluminescence and the intercrystalline boundaries of eight calcite crystals.

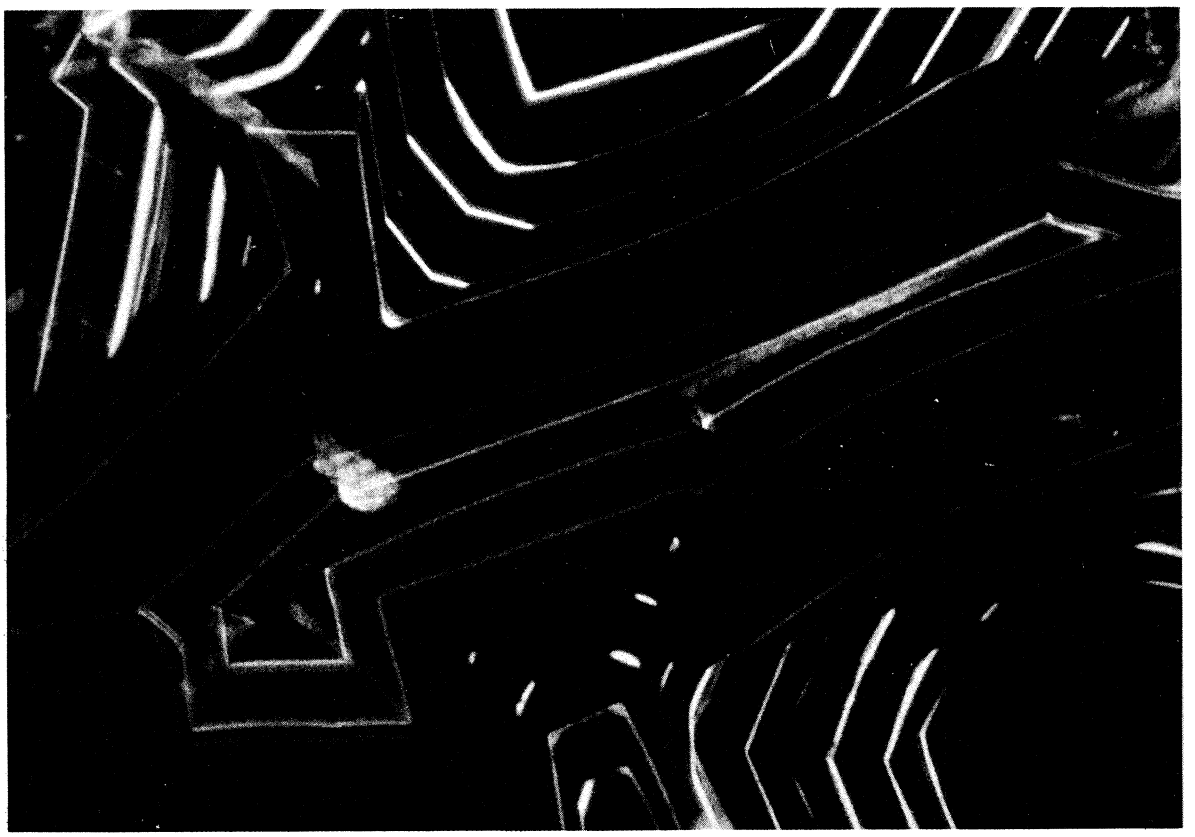

FIGURE 25. Cathodoluminescence photomicrograph of area shown in figure 24. The position of zones in figure 24 were constructed from this photomicrograph.

(*Facing p.* 496)

PHILOSOPHICAL TRANSACTIONS OF THE ROYAL SOCIETY A MATHEMATICAL, PHYSICAL & ENGINEERING SCIENCES

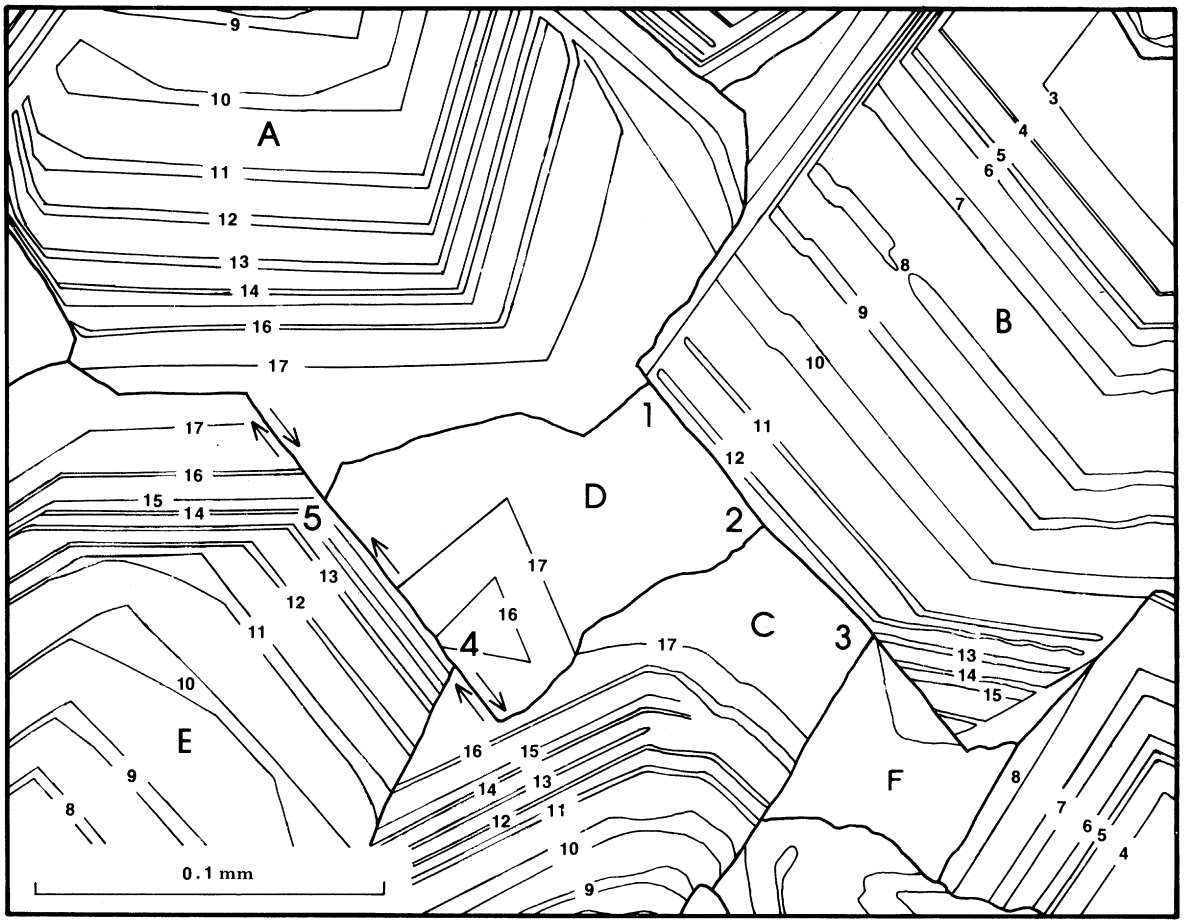

FIGURE 27. Inset area of figure 26B. Cathodoluminescent zones marked, chronologically, with small numbers. Intercrystalline boundaries are shown. Crystals are lettered. Enfacial junctions are marked with large numbers. The arrows close to 4 and 5 indicate relative direction of growth along the intercrystalline boundary.

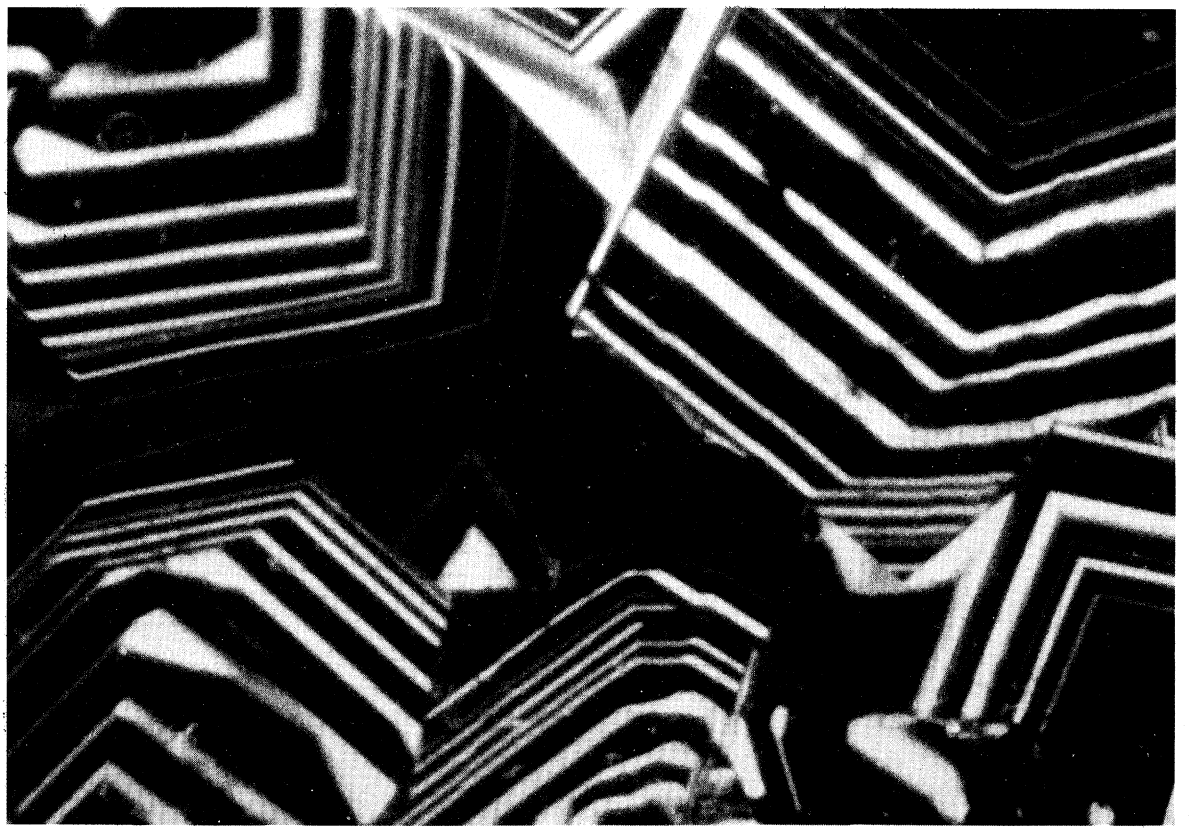

FIGURE 28. Cathodoluminescence photomicrograph of the area shown in figure 27. The position of zones in figure 27 were constructed from this photomicrograph.

PHILOSOPHICAL TRANSACTIONS OF THE ROYAL SOCIETY A MATHEMATICAL, PHYSICAL & ENGINEERING SCIENCES

Crystal C, figure 21, possesses one crystal face abutting an open void and is rooted on the pore wall. It is easy to assume that this crystal started growing where it is attached to the substrate and progressively becomes younger towards the void. However, examination of the same crystal in figure 23 shows that in *the plane of the section* the oldest part of the crystal is well away from the substrate and growth proceeded from this part both towards the pore and towards the substrate. Such a feature was described from the crystal growth diagrams.

The detailed arrangement between the fine zonation and intercrystalline boundaries is shown in figures 24 and 25, plate 1. The same zones from any pair of adjacent crystals meet precisely at the intercrystalline boundary, a situation demanded by impingement growth.

8. The problem of the enfacial junction

Enfacial junctions, regarded as one of the least equivocal criteria for the recognition of cements (Bathurst 1971, p. 425), are neither present in the graphical models of impingement growth nor in the examples of cement illustrated in figures 21–25. Yet Bathurst documents a high frequency of enfacial junctions (1971, table xvii) in cement as opposed to neomorphic calcite. The example of calcite impingement growth described in the last section displays only one enfacial junction out of 191 triple junctions measured. Is it possible that the cements measured by Bathurst (1971; Mississipian to Purbeckian age), by Fenninger (1968; Tithonian) and Di Girolamo (1968; Cretaceous) are not of the impingement type? An answer to this problem may be sought by examination of zoned spar exhibiting enfacial junctions. Such a rock is shown in figure 26 and figures 27 and 28, plate 2, which is very close to the example used by Bathurst (1971, figures 301–2) to illustrate enfacial junctions. The calcite spar occurs between the articulated valves of an ostracode. The ostracode occurs in a packstone containing pisoids (Wright 1981) which comes from the Llanelli Formation of Lower Carboniferous (Arundian) age, Blaen Onneu Quarry, South Wales. Ostracode valves are constructed of prismatic crystals (Scholle 1978) oriented normally to the valve surfaces. The clear spar attached to the inner surface of the two valves is optically and morphologically oriented normally to these surfaces. This indicates an epitaxial relation between the clear spar and ostracode test, although this cannot be seen with the optical microscope because the crystals are too small to resolve. Parts of the upper ostracode valve (figure 26A) are absent due to pressure solution along a stylolite (not shown in figure). The intercrystalline boundaries shown in figure 26A show a scattering of small crystals proximal to the ostracode valves and large, sometimes plane-bounded crystals distally. The presence of several unequivocal enfacial junctions is shown in figure 26 (arrowed). Examination by cathodoluminescence reveals that proximal growth commenced as many steep faced crystals (zone 1), which simplified rapidly to yield multiple zoned coarse spar (sixteen zones are present, of which six are shown in figure 26B).

An identical zonal pattern, or parts of it, can be recognized in all spar crystals within the ostracode. In this respect these crystals are similar to those from the Magnesian Limestone spar. However, a fundamentally different arrangement occurs between these two spar examples at the intercrystalline boundaries. Unlike the zones within the Magnesian Limestone spar, the zones within the 'ostracode fill' spar are not contiguous between adjacent crystals. Two types of discontinuity exist. In the first type, the intercrystalline boundary is parallel to the zones in one crystal, while the zones of the adjacent crystals intersect the boundary. An example of this type can be seen on figure 27 between crystals B, C and D, between triple junctions 1 and 3. In

PHILOSOPHICAL TRANSACTIONS OF THE ROYAL SOCIETY A MATHEMATICAL, PHYSICAL & ENGINEERING SCIENCES

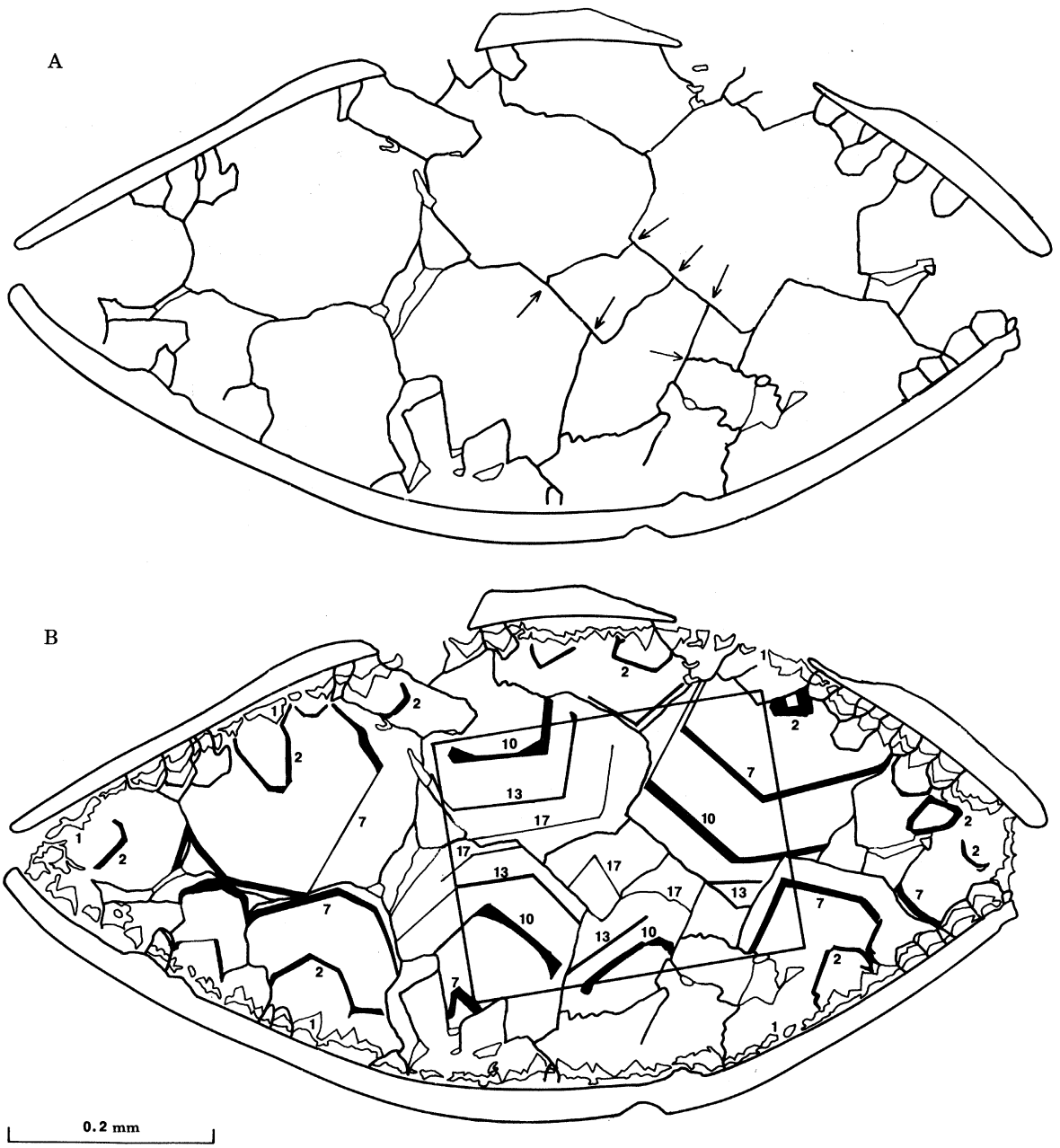

FIGURE 26. A. Line drawing showing intercrystalline boundaries of the calcite spar that fills the space between two ostracode valves. Thin section from Llanelli Formation (Arundian), Blaen Quarry, S. Wales. The positions of six enfacial junctions are arrowed. B. Same area showing the position of six most prominent cathodoluminescent zones.

the second type of discontinuity the zones from both crystals intersect the boundary at a high angle and exhibit offset. An example can be seen in figure 27 along the boundary between crystals C and E.

Bathurst (1964) proposed that enfacial junctions involved cessation of growth along one crystal face while the two encroaching crystals grow against the halted face. To support this hypothesis, Bathurst recorded the correspondence between the orientation of the halted face

(180° angle) and the orientation of known calcite crystallographic faces relative to the optic axis. The configuration of junction 2 (figure 27) agrees with Bathurst's proposal; one face in the series of zones in crystal B being parallel to the intercrystalline boundary. The age of crystals C and D when they reach the intercrystalline boundary is much younger (post zone 17) than crystal B (zone 12/12) at the boundary. However, this same intercrystalline boundary extends to include enfacial junctions 1 and 3 where a much more complex arrangement exists. The zones in crystals A and B, and crystals B and F all intersect the boundary. The time relation implied for junction 2 does not apply for junctions 1 and 3, for crystal B continued growth, until zone 16 towards crystal F. This anomalous time relation in crystal B is shown more dramatically with enfacial junctions 4 and 5, where the directions of growth along the intercrystalline boundary (arrowed in figure 27) in adjacent crystals, is in opposite directions (crystal A and E, and D and C). Two possibilities exist for the unusual relation between the zones and the intercrystalline boundaries, either portions of zones were never deposited, or the zones were deposited in a regular fashion but were later removed on a local basis.

With the first possibility, a step must have existed at these boundaries displaying offsetting of zones. This step (representing the zonal offset) developed on the crystal whose zones were more advanced into the available growth space. The step was overgrown as growth proceeded by the less advanced crystal, to become the intercrystalline boundary. The existence of such steps would require continued inhibition of growth on the step as it developed, while precipitation was proceeding normally next to the step. Wardlaw (1976) has described inhibition of dolomite growth on certain parts of crystals while other parts of the same crystal are growing. This inhibition is related to close proximity of other crystals, although Wardlaw admits that a completely satisfactory explanation for the small re-entrants and incompletely developed faces is still required.

The second possibility, the dissolution of material, readily explains the situation where a particular intercrystalline boundary shows no offset (zone 17, crystals C and D, figure 27), while the same zone shows considerable offset across an adjacent boundary (zone 17, crystals D and E, figure 27). The removal of material seems likely along the boundary now showing offset, the adjacent crystals moving together during or after dissolution. That intercrystalline boundaries act as conduits for fluid migration in the diagenetic environment is shown by the occurrence of fully cemented pores. At some stage during the centripetal growth of cement, each pore becomes isolated and unconnected to its neighbours except by access along the cement's intercrystalline boundaries. After this stage, continued growth implies continuity of access for fluids carrying calcium carbonate to precipitate the additional cement which eventually completely occludes the pores. If the zonal mismatches are caused by dissolution along the intercrystalline boundaries, then the amount of removal can be calculated from geometrical relations. If dissolution occurred repeatedly along particular boundaries during growth, then the earliest portions of crystals should show the greatest effects. Such an arrangement does not exist. The extent and occurrence of zonal offset is irregular, which implies dissolution was irregular spatially and perhaps temporally also.

The close approach of adjacent crystals required by the unusual type of growth described by Wardlaw (1976) is not found in the ostracode fill. The hypothesis that enfacial junctions are caused by such an unusual type of crystal growth therefore appears unlikely. While this mechanism cannot be ruled out, it is more likely that the majority of enfacial junctions are caused by modification of intercrystalline boundaries by dissolution. If this is the case, then these

PHILOSOPHICAL TRANSACTIONS OF THE ROYAL SOCIETY A MATHEMATICAL, PHYSICAL & ENGINEERING SCIENCES

boundaries can no longer be classified as impingement for they have been modified since formation.

Enfacial junctions also develop during growth where one generation of crystals terminates in crystal faces and is overgrown by another generation without epitaxy. Enfacial junctions will commonly arise along the contact between the two generations. This situation, however, should be readily recognizable and distinguishable from the type of enfacial junctions just described if zones are present.

9. Conclusions

The crystal growth diagrams presented here show how maturation occurs in a crystal aggregate as impingement growth proceeds from a plane, inert substrate into a void. An increase in crystal size develops, with a complementary decrease in crystal number, away from the substrate and a preferred orientation of both the crystals' longest axes and their g.g.vs normal to the substrate.

Rapid maturation occurs when component crystals have two (or few) g.g.vs whose magnitude far exceeds all other growth vectors. Slow maturation occurs if the crystals have many g.g.vs whose magnitude only slightly exceeds all other growth vectors.

The relation between the g.g.v. and the *c*-axis is important in distinguishing two optically different types of aggregate. During maturation length-fast crystals become dominant if the g.g.vs are coincident with the optic axes. If the g.g.vs are normal to the optic axis length-slow crystals develop. With calcite, true length-slow crystals cannot develop from a closed crystallographic form, because their g.g.vs are oriented at a high angle to (but never normal to) the *c*-axis.

The position, number and magnitude of the g.g.vs are controlled by the shape of the crystallographic form. The shape of the crystallographic form thus has an effect on the speed of maturation, yet eventually parallel crystals develop irrespective of the crystallographic form. Lindholm (1974) has correlated the $\{01\bar{1}2\}$ rhombohedron with fibrous calcite growth, and $\{40\bar{4}1\}$ rhombohedron with bladed growth, and the $\{02\bar{2}1\}$ and $\{05\bar{5}4\}$ rhombohedra with equant calcite. The modelling presented here indicates that such a correlation is invalid for mature impingement textures, also that $\{40\bar{4}1\}$ growth will produce columnar not bladed growth; bladed is a common misnomer, as pointed out by Logen & Semeniuk (1976).

The characteristics described for calcite aggregates also apply to other trigonal carbonates as they exhibit similar crystallographic forms. Dolomite, for instance, predominantly crystallizes as the equant $\{10\bar{1}1\}$ rhombohedron, so when this mineral forms impingement aggregates the mature stage will consist of length-slow crystals.

The style of textural maturation for any impingement aggregate, developed by the layer type of crystal growth from random nuclei on an inert substrate, may be predicted if the properties of the g.g.vs and the shape of the constituent crystals are known. A natural sequel to this work would be to use computer graphics to construct the crystal growth diagrams.

The recognition of the type of impingement growth modelled here is easiest when all stages of maturation are present. When growth occurs in spaces that are small, compared with the distance between nucleation points, recognition of impingement growth from an examination of the intercrystalline boundaries alone may be impossible.

The practice of using a list of textural criteria for the general recognition of all cements is best abandoned.

PHILOSOPHICAL TRANSACTIONS OF THE ROYAL SOCIETY A MATHEMATICAL, PHYSICAL & ENGINEERING SCIENCES

The cement from the Magnesian Limestone demonstrates that immature impingement growth cannot be recognized from the crystal growth diagrams, indeed this type of growth may never be recognizable if only the external features of the component crystals are considered. The calcite cement in this example has not changed in any gross way since it was deposited, indeed the process of cementation is still incomplete.

The second example, from the Llanelli Formation, shows possible cement that has grown epitaxially on the inner surfaces of ostracode valves. This example does not correspond to the crystal growth diagrams but was included to discuss the problem of enfacial junctions. These have developed either by a peculiar method of crystal growth or, more likely, as a result of dissolution. The generation of these enfacial angles probably took place during burial and resulted in the intercrystalline boundaries being modified away from the 3×120 triple junction of minimum grain boundary energy. This type of spar is probably much more frequent in the geological record than the impingement type exemplified here by the Magnesian Limestone.

The removal of calcite in the ostracode fill necessary to account for the zonal discontinuities and generate the enfacial junctions is considerable. If this calcite was removed by dissolution and redeposited, then late cements may, at least in part, have their source in the dissolution of earlier cements. Bathurst's (1971, table xvii) data on enfacial junctions shows them to be widespread and abundant in the cements of ancient limestones. If these junctions are created by intercrystalline dissolution, this process must have involved the transport of huge quantities of calcium carbonate. Such a process may affect the depositional framework to which the cement is attached, and if that is the case, then the unknown additional source sought by Bathurst (1971, p. 442) to supply $CaCO_3$ for cements may be found!

Without the inspired crystallography teaching of A. C. Bishop I received as an undergraduate this paper would not have been written. W. A. Cummins gave assistance on stereographic problems and D. B. Smith gave the Magnesian Limestone sample. The manuscript was improved by R. G. C. Bathurst, A. C. Bishop and I. J. Fairchild. Assistance was also received from the Geology Departments at Nottingham University, Louisiana State University and Cambridge Department of Earth Sciences.

References

Bathurst, R. G. C. 1958 *Lpool Manchr geol. J.* **2**, 11–36.
Bathurst, R. G. C. 1964 *Approaches to palaeoecology* (ed. J. Imbrie & N. D. Newell), pp. 357–376. New York: John Wiley & Sons.
Bathurst, R. G. C. 1971 *Dev. Sedimentol.* **12** (620 pages).
Bricker, O. P. 1971 *Carbonate cements*, p. 149. Baltimore-Maryland: John Hopkins Press.
Buckley, H. E. 1951 *Crystal growth* (571 pages). New York: Wiley.
Chilingar, G. V., Bissell, H. J. & Wolf, K. H. 1979 In *Dev. Sedimentol.* **25**A, 247–422.
Dickson, J. A. D. 1965 *Nature, Lond.* **205**, 587.
Dickson, J. A. D. 1978 *Geology.* **6**, 560–561.
Di Girolamo, P. 1968 *Boll. Soc. nat. Napoli.* **77**, 5–25.
Dunham, R. J. 1971 In *Carbonate cements, Johns Hopkins Univ. Studies Geology*, No. 19, 297–300.
Evamy, B. D. 1963 *Sedimentology*, **2**, 164–170.
Fairchild, I. J. 1980 *Sedimentology*, **27**, 631–650.
Fenninger, A. 1968 *Sedimentology*, **10**, 273–291.
Folk, R. L. 1965 In *Dolomitization and limestone diagenesis* (ed. L. C. Pray & R. C. Murray), *SEPM Spec. Pub.* 13, 14–48.
Folk, R. L. & Assereto, R. 1976 *J. Sed. Petrology*, **46**, 486–496.
Grigor'ev, D. P. 1965 Ontogeny of Minerals. (Ontogeniya Mineralov, 1961) (ed. Y. Brenner) (250 pp.). *Israel program for scientific translations*, Jerusalem.

PHILOSOPHICAL TRANSACTIONS OF THE ROYAL SOCIETY A MATHEMATICAL, PHYSICAL & ENGINEERING SCIENCES

Kendall, A. C. & Broughton, P. L. 1978 *J. Sed. Petrology*, **48**, 519–538.
Lindholm, R. C. 1974 *J. Sed. Petrology*, **44**, 428–440.
Logen, B. W. & Semeniuk, V. 1976 Dynamic metamorphism; processes and products in Devonian carbonate rocks, Canning Basin, Western Australia. *Geol. Soc. Australia Spec. Pub.* No. 6, 138 pages.
Palache, C., Berman, H. & Frondel, C. 1951 *Dana's system of mineralogy*. 7th ed., vol. 11 (1124 pages). New York: Wiley.
Schmidegg, O. 1928 *Jb. geol. Bundesanst., Wien* **78**, 1–52.
Scholle, P. A. 1978 *Memoir* **27**. *Am. Ass. Pet. Geol.* Tulsa, Oklahoma.
Schroeder, J. H. 1973 *Sed. Geol.* **10**, 179–204.
Sippel, R. F. & Glover, E. D. 1965 *Science, N.Y.* **150**, 1283–1287.
Smith, D. B. 1981 In *European fossil reef models*: Soc. Econ. Paleontologists & Mineralogists Spec. Pub. no. 30, 187–202.
Wardlaw, N. C. 1976 *Am. Ass. Pet. Geol. Bull.*, **60**, 245–257.
Wright, V. P. 1981 *J. Sed. Petrology*, **51**, 479–489.

PHILOSOPHICAL TRANSACTIONS OF THE ROYAL SOCIETY A MATHEMATICAL, PHYSICAL & ENGINEERING SCIENCES

PHILOSOPHICAL TRANSACTIONS OF THE ROYAL SOCIETY A MATHEMATICAL, PHYSICAL & ENGINEERING SCIENCES

FIGURE 25. Cathodoluminescence photomicrograph of area shown in figure 24. The position of zones in figure 24 were constructed from this photomicrograph.

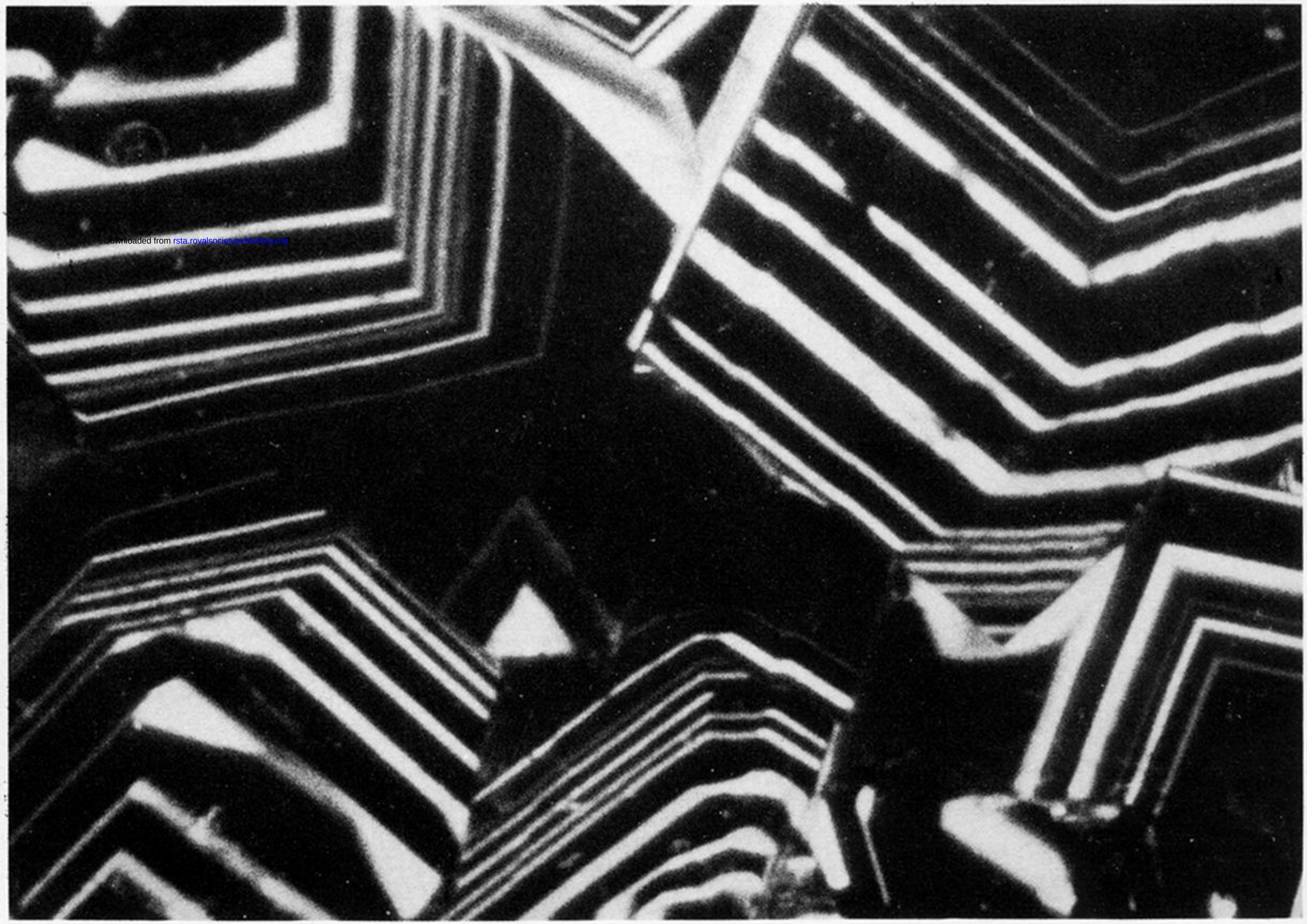

FIGURE 28. Cathodoluminescence photomicrograph of the area shown in figure 27. The position of zones in figure 27 were constructed from this photomicrograph.

PHILOSOPHICAL TRANSACTIONS OF THE ROYAL SOCIETY A MATHEMATICAL, PHYSICAL & ENGINEERING SCIENCES